University of Texas at El Paso
ScholarWorks@UTEP

Open Access Theses & Dissertations

2020-01-01

Design Of A Linerless Cryogenic Propellant Tank For A Small Payload Launch Vehicle

Itzel Adriana Torres
University of Texas at El Paso

Follow this and additional works at: https://scholarworks.utep.edu/open_etd

Part of the Mechanical Engineering Commons

Recommended Citation

Torres, Itzel Adriana, "Design Of A Linerless Cryogenic Propellant Tank For A Small Payload Launch Vehicle" (2020). *Open Access Theses & Dissertations*. 3049.
https://scholarworks.utep.edu/open_etd/3049

This is brought to you for free and open access by ScholarWorks@UTEP. It has been accepted for inclusion in Open Access Theses & Dissertations by an authorized administrator of ScholarWorks@UTEP. For more information, please contact lweber@utep.edu.

DESIGN OF A LINERLESS CRYOGENIC PROPELLANT TANK FOR A SMALL PAYLOAD LAUNCH VEHICLE

ITZEL A. TORRES

Master's Program in Mechanical Engineering

APPROVED:

Alejandra Castellanos, Ph.D., Chair

Jack Chessa, Ph.D.

Cesar Carrasco, Ph.D.

Stephen L. Crites, Ph.D.
Dean of the Graduate School

©Copyright

by

Itzel A. Torres

2020

to my

Family and Friends

who have supported me through the process

DESIGN OF A LINERLESS CRYOGENIC PROPELLANT TANK FOR A SMALL PAYLOAD LAUNCH VEHICLE

by

ITZEL A. TORRES

THESIS

Presented to the Faculty of the Graduate School of

The University of Texas at El Paso

in Partial Fulfillment

of the Requirements

for the Degree of

MASTER OF SCIENCE

Department of Mechanical Engineering

THE UNIVERSITY OF TEXAS AT EL PASO

May 2020

Acknowledgements

I would first like to pay my special regards to my advisor Dr. Alejandra Castellanos from the Mechanical Engineering Department at The University of Texas at El Paso, for her great advice, guidance, encouragement, and invaluable assistance that proved monumental in the success of this study. Additionally, I would like to thank the members of my committee Dr. Jack Chessa, Chair of Mechanical Engineering Department, and Dr. Cesar Carrasco from the Civil Engineering Department, both from The University of Texas at El Paso for their cooperation and expertise. I would also like to thank the Center for Space Exploration and Technology Research (cSETR) for all the oportunities and challenges that helped me grow. Thank you to Dr. Ashan Choudhuri, Luz Bugarin and Gloria Salas for providing me with all the resources I needed to thrive. A special thanks to Lucero Buendia who has been with me since I started this journey, it would not have been the same without you. Additionally, I would like to thank my parents, sister, and boyfriend for providing me with unfailing support, unconditional love, and encouragement throughout the process of researching and writing this thesis. Thank you and I love you. Lastly I would like to thank my friends, in no particular order: Noshin Habib, Hector Perez, Giovanna Perez, Monica Gabaldon, Zackery Nieto, Nathaniel Jurado and James Susen. This would have not been possible without your help and support, thank you.

Abstract

The need of lightweight launch vehicles that will reduce the cost and make flights more frequent into orbit has called for an increase of composite materials in the aerospace industry. Composite material's low thermal conductivity, high resistance to fatigue, and most importantly, low-weight can greatly reduce the cost of launch operations by decreasing the overall weight of the vehicle. Weight and cost savings are critical because any amount of weight that is saved can be directly applied as an additional amount of payload capability. The tanks on space vehicles are pressurized vessels that store fuel at cryogenic temperatures and have generally been either entirely manufactured or lined with metals. In most cases the tanks are the main structure of the vehicle which consequently can become the heaviest component. These vehicle tanks are exposed to extremely cold temperatures and gravitational loads that weaken the material and could potentially cause a fuel leak. Carbon fiber polymer matrix (CFRP) composite materials are a promising option for replacing conventionally used metal in cryogenic tank structures. Therefore, the understanding of composite materials under cryogenic exposure is essential for the next generation of spacecraft propellant tanks. The flexural behavior of plain-woven carbon fiber and plain-woven Kevlar fiber with Epon 828/ Epikure 3015 curing agent is studied as a potential commercially available material system for application in cryogenic tanks. Samples were exposed to cryogenic temperatures at one surface and to room temperature at the other surface to mimic a realistic environment that the tanks will be exposed to. Carbon and Kevlar fiber with epon/epikure material system for pressure vessels are an ideal material selection for cryogenic tank applications. Most current analysis only concentrate on testing materials entirely under cryogenic temperatures, or room temperature. Many fail to consider the small, but impactful temperature gradient caused by the low temperature propellant and ambient temperature on either side of the tank walls.

Table of Contents

Page

Acknowledgements v

Abstract vi

Table of Contents vii

List of Tables ix

List of Figures x

Chapter

1. Introduction 1

2. Material System 5

    2.1 Introduction 5

    2.2 Carbon Fiber Composites 5

    2.3 Fiber Orientation 6

    2.4 Matrix System 7

    2.5 Manufacturing Method 8

    2.6 Conclusion 8

3. Environmental Chamber 9

    3.1 Introduction 9

    3.2 Design 9

    3.3 Manufacturing 10

    3.4 Sample Placement 14

    3.5 Conclusion 18

4. Design of a Pressure Fed System with Textile Composites 19

    4.1 Introduction 19

    4.2 Material Selection 20

    4.3 Manufacturing 20

    4.4 Experiment 22

    4.5 Results 23

        4.5.1 Carbon Fiber Samples 24

        4.5.2 Kevlar Fiber Samples 28

    4.6 Conclusions 32

5. Matrix System 34
5.1 Introduction 34
5.2 Manufacturing 34
5.2.1 Method 1 35
5.2.2 Method 2 35
5.3 Testing 36
5.4 Conclusion 39
6. Centennial Small Payload Launch Vehicle Second Stage Composite Common-Bulkhead Tank 40
6.1 Introduction 40
6.2 Tank Calculations 41
6.3 Tank Thickness 42
6.4 Material and Weight 42
6.5 CAD Model 45
6.6 Conclusion 46
References 47
Appendix
A Commonbulkhead Tank Volume and Overall Dimensions 49
B Woven CF/EPON 828/EPIKURE 3015 51
C AS4/3501-6 (Axial) 53
D AS4/3501-6 (Transverse) 54
E AL 2219 T87 55
Curriculum Vitae 56

List of Tables

4.1 Carbon Fiber Room Temperature Samples 25

4.2 Carbon Fiber -60°C Samples 26

4.3 Carbon Fiber Temperature Gradient (-60°C/25°C) Samples 28

4.4 Kevlar Fiber Room Temperature Samples 30

4.5 Kevlar Fiber -60°C Samples 30

4.6 Kevlar Fiber Temperature Gradient (-60°C/25°C) Samples 31

5.7 Room Temperature Matrix Samples 38

5.8 -60°C Matrix Samples 39

6.9 Tank Properties 41

6.10 Material System Comparison 43

List of Figures

1 Five types of pressure vessels. Fowler, Calum P., et al. "Five types of pressure vessel for on-board gaseous fuel storage – Types I–IV are outlined in ISO 11439:2013; Type V is not currently covered by a standard or code (figure adapted from Ref. [12])." sciencedirect, 21 Dec. 2016, https://www.sciencedirect.com/science/article/pii/S0360319916330336 . . . 2

2 CAD model of a common-bulkhead tank design for helium, fuel and oxidizer volumes . . . 3

3 Unidirectional fibers running parallel to each other vs plain woven fibers braided together. Mark S. Mirotznik, et al. "Common weave architectures used in woven fabric structural composites. (a) 1-D unidirectional weave. (b) 2-D plain weave." semanticscholar, 2012, https://www.semanticscholar.org/paper/Broadband-Electromagnetic-Modeling-of-Woven-Fabric-Mirotznik-Yarlagadda/9b9c123b8e372a0c67f82a3bf21816c78676d4ae . . . 7

4 Environmental chamber design exposing samples to -60°C on one surface and to 25°C on the other . . . 10

5 Insulated foam box from Grainger . . . 10

6 Thermo Fisher Scientific TSU refrigerator to maintain an exterior environment of -60°C . . . 11

7 Environmental chamber trial 1 testing to test chamber's ability to insulate its interior . . . 11

8 Environmental chamber trial 2 testing to test chamber's ability to insulate its interior . . . 11

9 Chamber interior lined with a layer of polyurethane sheet foam insulation . . . 12

10 Environmental chamber interior is insulated for trial 3 to test ability to insulate its interior . . . 12

11 Heat source placed in insulated chamber interior and chamber wall view from cord and thermocouple incisions . . . 13

12 Environmental chamber interior is insulated and a heat source is integrated in trial 4 to test ability to maintain room temperature conditions . . . 13

13 Exterior surface of the sample is completely exposed while the opposing surface is only partially exposed through a slim incision 14
14 Trial results for configuration 1 on chamber's top surface 15
15 Exterior surface of the sample is only partially exposed while the opposing surface is completely exposed to the interior environment 15
16 Trial results for configuration 2 testing 15
17 Configuration 3 samples are completely exposed to interiror environment . . 16
18 Configuration 3 samples are completely exposed to exterior environment . . 16
19 Test results from configuration 3 samples 17
20 Long exposure trial testing with configuration 3 sample testing for 4 hours and 40 minutes 17
21 Environmental chamber final design with samples positioned using configuration 3 18
22 VARTM process illustrating layers inside vacuum bag 21
23 Laminate manufacturing using VARTM method before and after resin infusion 21
24 Kevlar and carbon laminates after samples were water jet cut and removed . 22
25 Flexural three-point bending test setup. The sample is placed between two supports and the load is applied at the center 23
26 Carbon fiber samples during three-point bending test 24
27 Kevlar fiber samples during three-point bending test 24
28 Stress - Strain graph of carbon fiber samples tested at room temperature . . 25
29 Microscope view of carbon fiber room temperature failure mechanism 25
30 Stress - Strain graph of carbon fiber samples tested at -60°C 26
31 Microscope view of carbon fiber -60°C failure mechanism 26
32 Stress - Strain graph of carbon fiber samples tested at -60°C/25°C 28
33 Microscope view of carbon fiber temperature gradient failure mechanism . . 28
34 Stress - Strain graph of Kevlar fiber samples tested at room temperature . . 29
35 Microscope view of Kevlar fiber room temperature failure mechanism 29
36 Stress - Strain graph of Kevlar fiber samples tested at -60°C 30
37 Microscope view of Kevlar fiber -60°C failure mechanism 31
38 Stress - Strain graph of Kevlar fiber samples tested with -60°C / 25°C temperature gradient 32

39 Microscope view of Kevlar fiber -60°C / 25°C temperature gradient failure mechanism 32
40 3D printed cast resin molds for sample manufacturing 35
41 Method 1 resin sample with visible air bubbles on its surface 36
42 Sample comparison of Method 1 sample (left) and Method 2 sample (right). Method 2 sample shows little to none air bubbles. 36
43 Flexural testing of the resin samples 37
44 Stress - Strain graph results of resin room temperature samples 38
45 Stress - Strain graph results of resin -60°C samples 39
46 Strength vs Stiffness graph compares three different material systems 44
47 Helium Tank 45
48 Fuel Tank 45
49 Oxidizer Tank 45
50 Complete assembly of commonbulkhead tank 46

Chapter 1

Introduction

The growing market for small payloads created a need for more frequent, low-cost launches. Space launches are very costly, and the main driving factor for this is dependent on the weight. Propellant tanks, or pressure vessels, are the main structural component of the vehicle and have a direct impact on the overall weight. Their design is crucial to the efficiency and safe operation of the system. Their design is heavily dependent on the propellant choice, payload requirement, tank material and manufacturing process. A substantial reduction in vehicle structural weight will rely on the development of new technologies, materials and process techniques. [1] describes the different categories for pressure vessels which are: Type I – all metal, Type II – partially overwrapped metallic tanks, Type III – composite overwrapped structure lined with metal, Type IV – composite overwrapped structures lined with a polymer, and Type V – all composite. A problem with current tanks is the liners are not mass efficient. Metal liners are only used to prevent propellant leaks and do not provide any structural support. Liners are overdesigned due to the fact that they are designed to bursting pressure instead of leakage. This is detrimental to the weight of the vehicle. Part of the problem is the liner and tank materials are different and have different thermal expansions. The use of Type V pressure vessels can eliminate these problems, but the ones that have been manufactured have experienced lowered strain than planned, leakage, or not a significant difference from metal lined tanks.

Metallic alloys are the current material choice for cryogenic tanks. These high fracture toughness and high strength materials demonstrate damage resistance, in spite of the extreme operating conditions. The manufacturing process and development costs for these alloys are relatively low. This is due to the well-established process for metallic pressure vessels and general knowledge of the material behavior. However, despite all their advantages, metallic alloys remain a relatively high-weight solution [2]. These types of tanks are generally composed of layers of insulation with some type of metal liner exposed to extremely cold temperatures in their interior and to ambient temperatures on their external surface. A large temperature gradient across the wall thickness will cause thermal expansion and contraction in the tank walls. This will result in an uneven expansion or contraction of the material. If the stresses exceed the strength of the material, cracks will initiate and propagate through

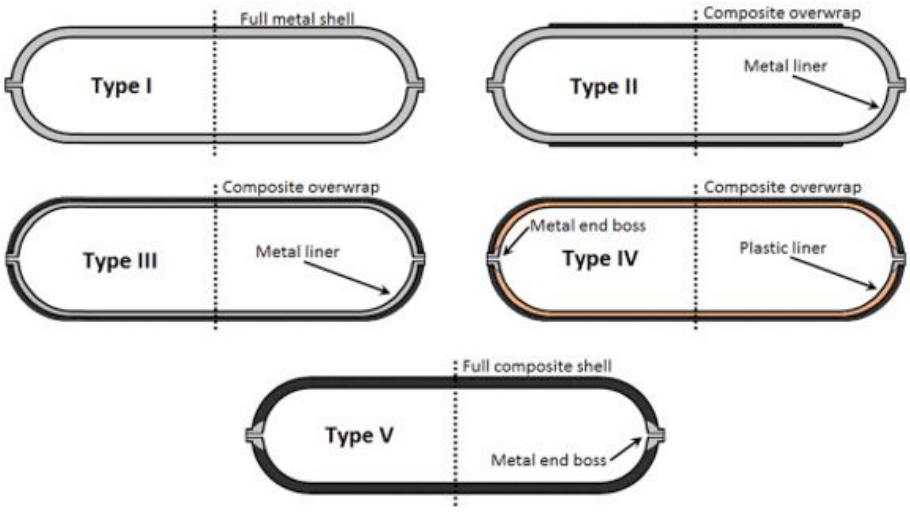

Figure 1: Five types of pressure vessels. Fowler, Calum P., et al. "Five types of pressure vessel for on-board gaseous fuel storage – Types I–IV are outlined in ISO 11439:2013; Type V is not currently covered by a standard or code (figure adapted from Ref. [12])." sciencedirect, 21 Dec. 2016, https://www.sciencedirect.com/science/article/pii/S0360319916330336

the path of least resistance [3]. Developments in material science have allowed engineers to contemplate the use of all composite linerless tanks, an alternative less traditional material method in cryogenic pressure vessel design. [4] In contrast to metal lined vessels, linerless composite tanks depend on the composite shell itself to behave as a permeation barrier in addition to carrying all pressure and environmental loads. Linerless composite tanks for in-space propulsion are required to be highly optimized structures. These tanks must be as impermeable and strong as metal lined tanks while significantly reducing their weight. Many factors can be attributed toward the fracture and failure of composite materials. The material system selected and the manufacturing method will affect its mechanical properties. Manufacturing methods can introduce defects and determine the fiber volume fraction of the system. The main concern for the use of composite materials in cryogenic pressure vessels is matrix microcracking. This is the first failure mode in composites. The matrix's coefficient of thermal expansion is one order of magnitude larger than the fiber's causing it to expand at a much faster rate. Unidirectional carbon fiber–reinforced composites have been widely utilized in the aerospace industry because of their great mechanical properties. Still, the strength in the thickness, transverse, direction of the fibers is a restrictive design factor. There are no fibers oriented in this direction to endure transverse loads. The flexural

failures are due to the weak performance of the material system in the transverse direction [5]. Substituting woven for unidirectional fibers can provide endurance for the transverse loads and offer resistance to the initiation and propagation of matrix microcracks. In order to improve payload capabilities and launches into suborbital, orbital or interplanetary space it is necessary to attain very low vehicle mass fractions. In an effort to further reduce the weight of the vehicle the tank configuration can also be a factor. [6] created a novel fuel structure for cryogenic fuels in an aerospace vehicle. The aluminum tank is comprised of different containers with volumes separated by common wall bulkheads to minimize the tank surface area. Pressure fed systems are usually composed of a fuel, oxidizer, and pressurant gas tank. The three tanks can be combined into one, separating their contents by sharing a common bulkhead wall. The use of composite materials and a common-bulkhead configuration can greatly further reduce the dry mass fractions of the vehicle.

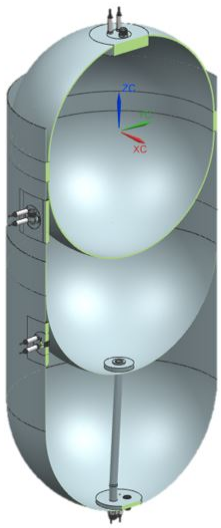

Figure 2: CAD model of a common-bulkhead tank design for helium, fuel and oxidizer volumes

Propellant tanks on spacecraft vehicles are subjected to a variety of extreme temperatures in the range of -170°C to 200°C. They are also exposed to ultra violet attacks, outgassing, thermal fatigue and atomic oxygen that could potentially lead to a fuel leak [7]. The materials used must be able to withstand the extreme cryogenic temperatures, operational loads for take-off, and gravitational forces that a launch into space presents. Aerospace industries utilize carbon fiber reinforced epoxy composites for their structural components because of their low thermal conductivity, high resistance to fatigue, and the opportunity of selecting

an optimum laminate lay up for a specific application [8]. With today's increased use of composite materials, all-composite linerless propellant tanks are a way to reduce these high mass fractions while simultaneously providing a strong material. The understanding of composite materials microcracking and damage propagation under cryogenic exposure is essential for the next generation of spacecraft propellant tanks to improve design optimization and minimize weight in these structures. In this study, flexural properties of plain woven carbon and plain woven Kevlar with Epon 828/Epikure 3015 material system are evaluated through flexural testing using a crosshead rate speed of 1 mm/min. To mimic a realistic scenario one surface of the sample is exposed to an environment of -60°C while the other side is kept at ambient temperature.

Chapter 2

Material System

2.1 Introduction

The success of an all composite linerless cryogenic tank is greatly dependent on its material system. Matrix microcracking is the first mode of failure in composites. This is due to the fact that fiber and matrix have different coefficients of thermal expansion. The matrix's coefficient of thermal expansion tends to be an order of magnitude greater than the fibers', meaning it will expand or contract at a much faster rate. While there are many different material systems that have been successful in cryogenic pressure vessels not all are explicitly known or commercially available. Some patents choose to define their material system as only "fiber reinforcement and highly ductile resin" not specifying a certain material system. Others do specifically list the material system used, but are not commercially available to purchase. Selecting a material system for this study was crucial for its success. Composite materials properties are dependent on many aspects: the fiber material, the matrix, and the manufacturing method. The goal of this study is to find a commercially available material system to utilize in the design of a cryogenic common-bulkhead tank.

2.2 Carbon Fiber Composites

Carbon fiber reinforced resin matrix composite materials are utilized in the aerospace industry because of their high stiffness-to-weight ratios, high tensile strength, high chemical resistance and low thermal conductivity. Carbon fiber composites are five times lighter than grade 1020 steel, yet five times stronger [9]. Many studies have been performed on various carbon fiber and matrix material systems to study their behavior at certain environmental temperatures and loads. [10] performed dynamic mechanical analysis on CFRPs that had been exposed to -40°C for 0, 30, 45 and 60 days to test the influence of low temperature exposure on their mechanical properties. Flexural tests were conducted on an Instron 3382 Universal Testing Machine with a crosshead speed set at 2 mm/min. The specimens material system consisted of carbon fabric C400P (TR50S) Plain Weave and resin R2940 and had a stacking sequence of $[(0/90)2/\pm45]$s. The study proved the deterioration of static bending modulus and bending strength. It was observed the storage modulus was also reduced

as the time of exposure increased, while there was an increase in the loss modulus versus time of exposure. It is especially important to study the behavior of these composites in a large temperature range because of the exposure pressurized cryogenic vessels experience. Tanks are subjected to cryogenic temperatures from the interior and to ambient temperatures at their exterior. [3] determined the thermo mechanical responses of plain weave carbon fiber with reinforced Kevlar fiber tows and Epon 862/Epikure 9553 hardener matrix material when exposed to cryogenic temperatures. Flexural and tensile tests were conducted on the samples after they were submerged into a liquid nitrogen tank at -196°C for six hours. The results showed that exposure to cryogenic temperatures had no significant influence on tensile chord modulus, tensile strength, or flexural properties when compared to samples that had not been subjected to cryogenic temperatures. The fiber properties are not significantly influenced by the temperature changes, but the matrix is. As temperatures drop matrix materials become more brittle, and are subject to microcracking. [11] evaluated carbon fiber reinforced plastics (CFRP's) for their applicability as cryogenic composite tanks. The materials tested consisted of different types of epoxy, bismaleimide, and PEEK based matrices with intermediate modulus/standard carbon fiber. Static tensile and interlaminar fracture toughness testing inside the environmental chamber revealed that under cryogenic temperatures matrix cracks occur at lower mechanical loads and toughness increases.

2.3 Fiber Orientation

Fiber orientation influences structural behavior and mechanical performance. Unlike isotropic materials, like metals, composites have directional strength properties. The properties are dependent on the layout of the fiber and the proportion of the fibers in relation to the matrix [9]. Unidirectional fibers lay flat and run in a single, parallel direction. There is no cross-section weave to divide the fiber strength. The concentrated density of fibers provides maximum longitudinal tensile strength in the direction of the fiber. However, unidirectional fibers are weak in the transverse direction. The much weaker matrix system must carry the load, but while a high-strength fiber can have a tensile strength of 3500 MPa or more, a typical matrix generally has a tensile strength of only 35 to 70 MPa [12]. The parallel nature of the fibers allows crack propagation along the matrix that can lead to failure. Woven fabrics are shaped by interlacing fibers in a regular pattern or weave style. The fabric has good stability and is symmetrical. Woven fibers provide a barrier to prevent leakage,

offer resistance to the initiation of microcracks and to crack propagation. Fig. 3 illustrates the difference between unidirectional and woven fibers. Plain woven carbon fiber was chosen for this study as tanks are exposed to a variety of loads and pressures, in the axial and transverse direction.

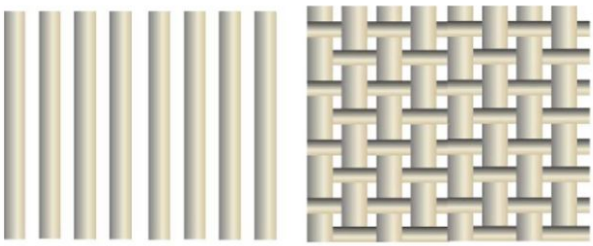

Figure 3: Unidirectional fibers running parallel to each other vs plain woven fibers braided together. Mark S. Mirotznik, et al. "Common weave architectures used in woven fabric structural composites. (a) 1-D unidirectional weave. (b) 2-D plain weave." semanticscholar, 2012, https://www.semanticscholar.org/paper/Broadband-Electromagnetic-Modeling-of-Woven-Fabric-Mirotznik-Yarlagadda/9b9c123b8e372a0c67f82a3bf21816c78676d4ae

2.4 Matrix System

The matrix is a polymer resin, such as epoxy, that binds the fibers together. There are many different types of matrix material systems with different mechanical properties. When the matrix is exposed to cryogenic temperatures it will become more brittle and can initiate microcracking. Shrinkage may occur for certain types of resins after curing, this can lead to delamination in the fibers. Certain systems may cure at room temperature or may need an autoclave. Epon 828 resin purchased from HEXION was chosen for this study. As the technical datasheet specified when hardened with the appropriate curing agent, Epikure 3015 hardener, very good mechanical, adhesive, and chemical resistance properties are obtained. This commercially available resin material system provided good material properties for cryogenics, small amount of shrinkage after curing, and the ability to cure at room temperature after 16 hours or after 2 hours at 93°C [13].

2.5 Manufacturing Method

The manufacturing method chosen for composite materials is important. Manufacturing defects may be introduced into the composite which can contribute to its failure. An important factor affected by manufacturing method is fiber volume fraction, or the percentage of the fiber volume in the entire fiber-reinforced composite material. Using the vacuum assisted resin transfer molding (VARTM) method around a 0.45 to 0.5 fiber volume fraction can be achieved. VARTM is a fabrication method that attaches a vacuum bag to the top of a mold and applies vacuum to create the continuous flow of infused resin from one side of the mold to the other. The use of an autoclave can result in up to a 0.7 fiber volume fraction because of the full pressure it is exposed to. An autoclave is a strong heated container that utilizes high pressure and high temperature processes. There is also the hand lay-up process, which is a molding process where fiber reinforcements are placed by hand then wet with resin. Most tank manufacturing processes use filament wounding, in which the dry fibers are impregnated with resin, wound onto a mandrel, and cured with an autoclave.

2.6 Conclusion

The goal of this study was to find a commercially available material system to utilize in the design of a cryogenic pressure vessel. Carbon fiber reinforced matrix composite materials were chosen for their exceptional mechanical properties. Woven carbon fibers will provide a barrier to prevent microcracking. The matrix material system consisting of Epon 828 with Epikure 3015 hardener provides good qualities under cryogenic temperatures. Its consistency allows for the VARTM process as a manufacturing method. The resin's ability to cure at room temperature does not require the use an autoclave. The mechanical properties of plain-woven carbon fiber with Epon 828 resin and Epikure 3015 hardener material system will be evaluated for their potential application in a cryogenic tank.

Chapter 3

Environmental Chamber

3.1 Introduction

The purpose of creating an environmental chamber for sample testing was to be able to expose one sample to two different environments simultaneously. Material samples tend to be tested at either room temperature or at low temperatures to obtain their material properties. Materials used in propellant tanks are exposed to cryogenic temperatures on one surface and ambient temperatures on the other. This creates a temperature gradient within the sample. In order to simulate a temperature gradient, it was important to have the sample expose either surface to these two constant very different environments. As materials exposed to cold temperatures tend to become more brittle, the material properties of the sample might vary on either surface and its fracture mechanism may be affected. Studying the effect of temperature gradients in composite materials is important in future propellant tank design.

3.2 Design

The two environments for testing included -60°C and room temperature. One sample required to have either surface exposed to each temperature simultaneously. When deciding on the design of the chamber a big factor was determining how to maintain either side exposed to these temperatures for an extended period of time. The idea was to create an enclosed chamber and place the sample in a way that only one surface would be exposed to the chamber interior. Then, by placing the chamber inside an environmental fridge, the outer surface of the sample would be exposed to a constant environment of -60°C. In order to maintain the inside of the chamber at room temperature a temperature-controlled heat source was included to prevent the temperature from falling to -60°C. It was more efficient and required less power to incorporate a heating source inside, rather than trying to cool the inside uniformly to such low temperatures.

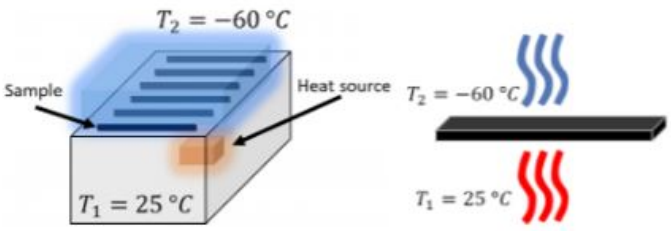

Figure 4: Environmental chamber design exposing samples to -60°C on one surface and to 25°C on the other

3.3 Manufacturing

The environmental chamber was manufactured using a highly insulated foam box. An insulated shipping box was purchased from Grainger. Its dimensions were 1.5 in thick walls with a height and width of 13 in by 13 in. It included a removable lid which was also 1.5 inches thick.

Figure 5: Insulated foam box from Grainger

In order to condition the temperature gradient samples, the feasibility of maintaining one sample's opposing surfaces at different environments simultaneously had to be proved. Trials 1 and 2 were conducted without using a sample to determine how well the chamber could maintain room temperature conditions in its interior. Thermocouples were placed inside and outside the chamber to monitor the temperature. The chamber's lid was taped down to prevent any leaks and placed into an environmental fridge at -60C.

Fig. 7 and Fig. 8 illustrate the behavior of the chamber's interior and exterior tempera-

Figure 6: Thermo Fisher Scientific TSU refrigerator to maintain an exterior environment of -60°C

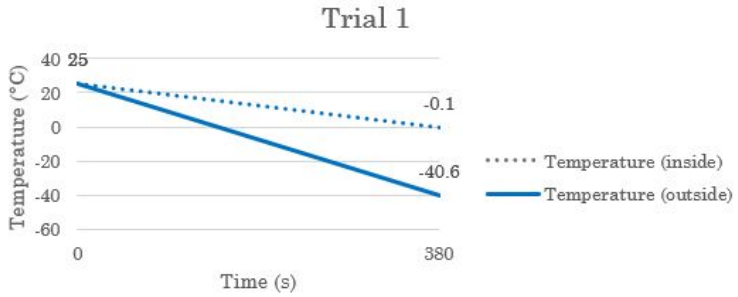

Figure 7: Environmental chamber trial 1 testing to test chamber's ability to insulate its interior

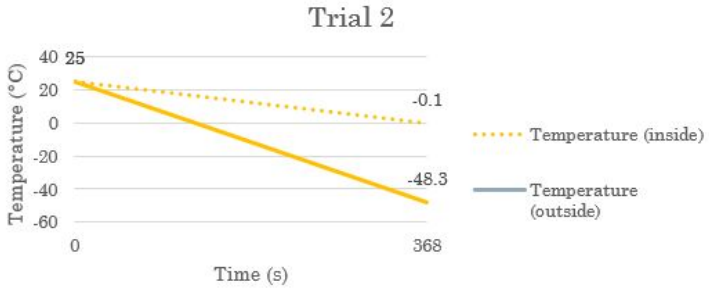

Figure 8: Environmental chamber trial 2 testing to test chamber's ability to insulate its interior

tures. Both trials were run for about 6 minutes and displayed the same behavior. Interior and exterior temperatures began to drop immediately after being placed in the environmental fridge. The chamber was able to maintain a temperature difference of about 40°C between the interior and exterior. While the chamber did sustain a large delta T, the interior temperature dropped into negative values and did not remain at room temperature for longer than a minute. This would not provide a constant room temperature environment in which to condition a sample. In order to preserve room temperature conditions for a longer period of time, the interior of the chamber was lined with a layer of polyurethane sheet foam insulation. Once more, the chamber lid was taped down and then placed inside the environmental fridge to begin Trial 3.

Figure 9: Chamber interior lined with a layer of polyurethane sheet foam insulation

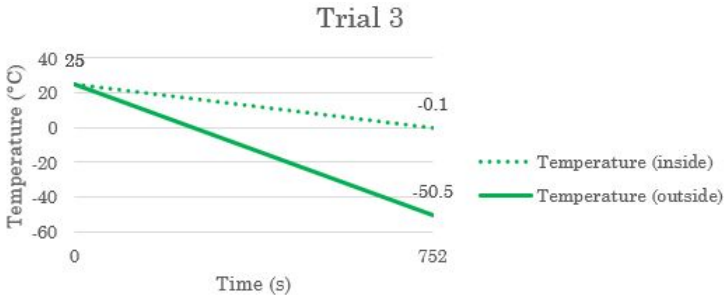

Figure 10: Environmental chamber interior is insulated for trial 3 to test ability to insulate its interior

Fig. 10 displays the temperature behavior of trial 3. The duration of this trial was 12 minutes. Again, both temperatures began to steadily drop after being placed in the environ-

mental fridge and the interior temperature dropped into negative values. The polyurethane insulation prevented the temperature from dropping as quickly, it took twice as long to reach the same temperature as trials 1 and 2. Nevertheless, the interior was not able to maintain room temperature conditions for an extended period of time. For Trial 4 a thermo-controlled heat source, a heating pad, was integrated into the interior of the chamber. Several more layers of polyurethane insulation were used to fill the remaining space in the chamber in order to elevate the heat source and place it near the top surface where the samples would be placed. A small perforation was made on the side of the chamber in order to insert the heater's extension cord. This same perforation was used to introduce thermocouple cables as well and insulative double sided tape was placed around the perforation to prevent leaks.

Figure 11: Heat source placed in insulated chamber interior and chamber wall view from cord and thermocouple incisions

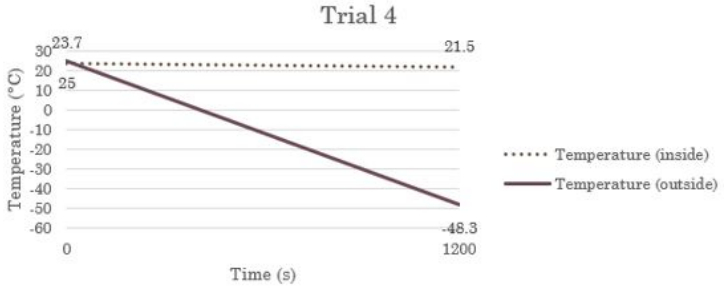

Figure 12: Environmental chamber interior is insulated and a heat source is integrated in trial 4 to test ability to maintain room temperature conditions

The chamber lid was taped down and placed into the environmental fridge. Based on the results from previous trials, the interior temperature would begin to drop immediately after being placed in the environmental fridge. To prevent this from happening, the heating

pad was turned on before beginning the trial and adjusted accordingly to maintain the temperature at 23° +/- 2°C during the trial. Trial 4 had a duration of 20 minutes. As displayed in Fig. 12, the chamber was able to maintain an interior temperature of 21°C for 20 minutes while the exterior temperature continued to drop. This proved that the chamber would be capable of exposing and maintaining a sample at two separate environments.

3.4 Sample Placement

Trial 4 proved the chamber's ability to maintain room temperature conditions in its interior while exposed to a -60°C environment. The next step was to incorporate the samples into the chamber's top surface, or lid, to condition them. In order to ensure the samples would be in a position that would allow them to expose either surface to each environment, three different configurations were tested. Configuration 1 placed the sample in a position where one surface was completely exposed to the cold environment while only a small incision on the opposing surface of the lid exposed it to room temperature conditions as shown in Fig. 13. Thermocouples were placed on either surface of the sample to monitor its temperature during the trial. The trials for sample configuration testing focused on monitoring the sample temperature, as opposed to the previous trials that only monitored the temperature of the environment inside and around the chamber.

Figure 13: Exterior surface of the sample is completely exposed while the opposing surface is only partially exposed through a slim incision

The sample was placed on the lid using configuration 1, the lid was taped down, and the chamber was placed in the environmental fridge to begin the trial. The heating pad temperature was adjusted accordingly throughout the test to maintain room temperature conditions inside the chamber. Fig. 14 shows the results from configuration 1 testing. After

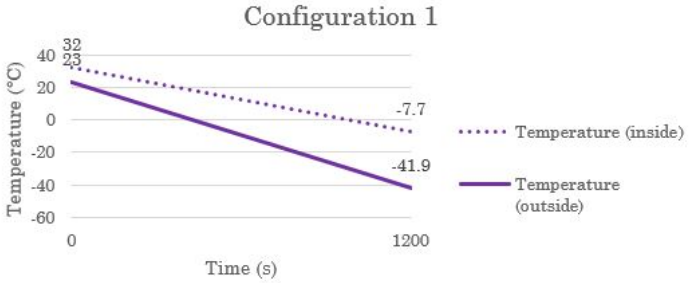

Figure 14: Trial results for configuration 1 on chamber's top surface

20 minutes the sample displayed a 34.2°C temperature gradient between its two surfaces. Configuration 2 is the inverse of configuration 1. This configuration positions one surface of the sample to be completely exposed to the interior room temperature environment while only a small incision on the opposing surface of the lid is exposed to -60°C. The same procedure was followed as for previous trials and the sample's surface temperatures were recorded.

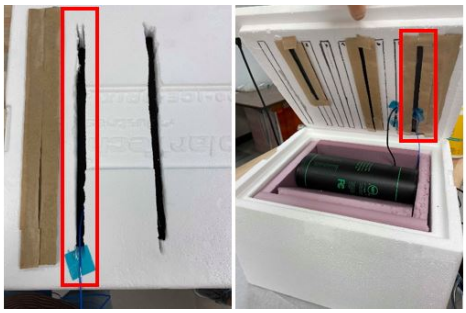

Figure 15: Exterior surface of the sample is only partially exposed while the opposing surface is completely exposed to the interior environment

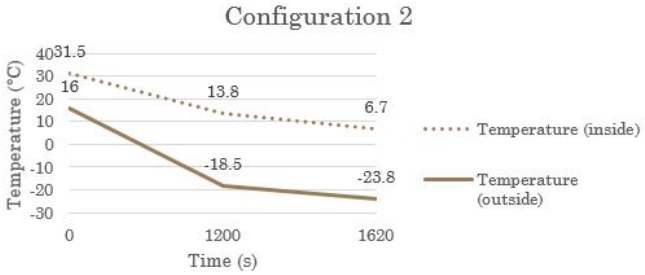

Figure 16: Trial results for configuration 2 testing

The trial for configuration 2 was run for 27 minutes and the sample achieved a 30.5°C temperature gradient between surfaces. After 20 minutes both interior and exterior temperatures began to stabilize. Configurations 1 and 2 had been considered to attempt a sample placement that did not require a large incision in the chamber that could cause a leak. The results proved that even with various incisions the chamber was able to maintain a temperature gradient in the samples, but the positions that were partially exposed were not representative of an actual propellant tank's environment exposure. For configuration 3, an incision a bit larger than the samples was made, this thoroughly perforated the thickness of the lid. In order to prevent leaks, the sample was wrapped in insulative double sided tape around the edges and wedged into the lid perforation. Another layer of insulative double sided tape was placed above and below the sample. In this configuration, the sample's surfaces were equally exposed to the interior and exterior environments. The chamber lid was taped down, the heat pad was adjusted, and the chamber was placed inside the environmental fridge for testing. The trial was run for 56 minutes and the sample temperature reached equilibrium, interior and exterior temperatures stabilized, after about 24 minutes. The sample had a temperature gradient of 34.5°C between its surfaces.

Figure 17: Configuration 3 samples are completely exposed to interiror environment

Figure 18: Configuration 3 samples are completely exposed to exterior environment

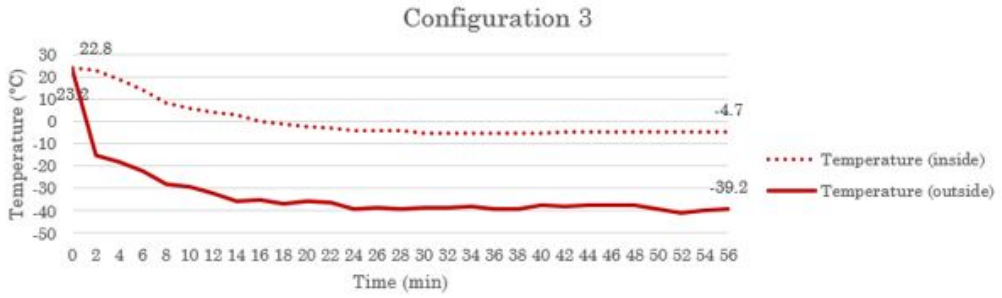

Figure 19: Test results from configuration 3 samples

Configuration 3 was the most realistic scenario to which materials are exposed to in propellant tank applications. Using configuration 3, a long exposure test was performed. This test was to define if the chamber could maintain the sample exposed to two environments for an extended period of time. The heating pad could only be active for 5 hours to give accurate readings and to prevent malfunctions. Thermocouples were placed on either surface of the sample and the long exposure trial was run for 4 hours and 40 minutes. Fig. 20 shows the results from the long exposure trial. The sample had a temperature gradient of 8°C between its surfaces and the temperature stabilized after about 40 minutes. The final design of the chamber utilized configuration 3. Eight equally spaced samples were placed on the lid as shown in Fig. 17 and Fig. 18. All samples were traced and evenly distanced to prevent them from having contact with each other, as this could affect the results, and to ensure the weight did not cause the chamber to collapse onto itself.

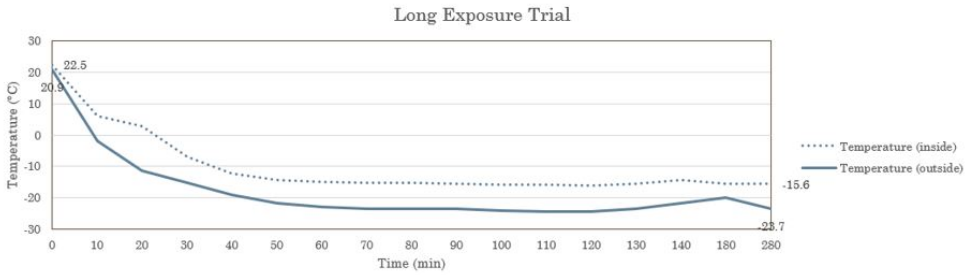

Figure 20: Long exposure trial testing with configuration 3 sample testing for 4 hours and 40 minutes

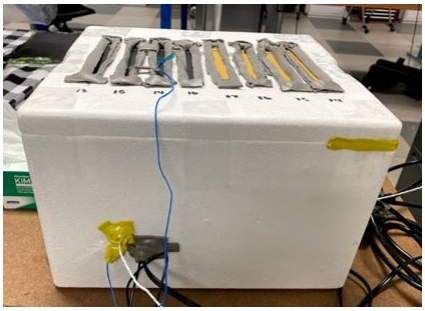

Figure 21: Environmental chamber final design with samples positioned using configuration 3

3.5 Conclusion

Based on the results of the trials, it was concluded that the chamber could in fact maintain a significant temperature gradient within the sample by exposing it to different environments simultaneously. The longer the trial was run, the smaller the temperature gradient became. The final chamber design consisted of its interior insulated with polyurethane sheet foam and a thermo-controlled heat source placed inside. The only incisions in the chamber walls were for the heat source and thermocouple cords. Configuration 3 was the most realistic in exposing the samples to room temperature conditions on one surface and to a -60°C environment on the other. Three layers of insulative tape were used on the samples and the lid was taped down onto the chamber walls to prevent leaks. The success of the chamber leads to future work on exposing a sample to cryogenic and room temperature conditions with the use of liquid nitrogen to study its temperature gradient.

Chapter 4

Design of a Pressure Fed System with Textile Composites

4.1 Introduction

Recently there has been a significant rise in space exploration with increases in missions that plan to recover samples, re-fuel in space and return to earth. These missions are more demanding on the propulsion system which in return increase the mass of the vehicle. A spacecraft's main limiting factor is its weight. The heavier it is, the more costly the mission will become. The tanks are the largest structural component of the vehicle. Usually these tanks are made of aluminum or steel and are run with a pump-fed system. Replacing pump-fed by a pressure-fed system makes the system very simple, reducing the probability for error. Pressure fed systems require high pressures, which make the tanks heavy and result in very high dry mass fractions. Substituting aluminum/steel tanks with composite materials can result in significant weight savings. NASA has already worked on the Composite Cryotank Technology Demonstration (CCTD) Project in which they designed and built a composite liquid-hydrogen cryogenic tank that saved 30% in weight and 25% in cost compared to a state-of-the-art aluminum metallic cryogenic tank [14]. Most tanks today are either entirely metal or contain a metal/polymer liner wrapped in composite material. The purpose of the liner is only to prevent leaks, it does not provide structural support. Eliminating the liner can reduce cost, manufacturing time and a major portion of the tank mass. [4] illustrates how a linerless all-composite tank can reduce total tank mass, increase efficiency and therefore provide the most efficient storage vessels for in-space propulsion systems. Carbon fiber composites are a promising material because of their low thermal conductivity, high resistance to fatigue and ease of manufacturing into complex forms with fewer fasteners required. The only concern for composite pressure vessels is their permeability, exposure of these tanks to cryogenic temperatures and high pressures can affect the strength and fracture mechanism of the material as they become more brittle, and could lead to a fuel leak. Matrix microcracking is usually the first failure mode in composites. Another factor in the tank's permeability is the fiber lay-up. Most tanks use unidirectional fibers that are wound round the tank and held together by the matrix system. This fiber layup can facilitate microcrack propagation through the tank. [1] found that braided or woven-fiber plies provide protection against the

propagation of manufacturing flaws, voids and resin microcracks when a composite pressure vessel is subjected to pressure cycles during operation. Using many formations of braided- or woven-fiber plies can lead to a desirable barrier performance. An all composite linerless pressure vessel is possible incorporating the use of highly ductile resin material and a braided or woven-fiber reinforcement. Understanding the behavior of woven-fiber and matrix material systems is critical in the design for a linerless composite cryogenic pressure vessel. This study concentrates on the flexural behavior of a commercially available material system: plain-woven carbon fiber and plain-woven Kevlar fiber with Epon 828/ Epikure 3015 curing agent for their potential application in cryogenic tanks.

4.2 Material Selection

The material selection for this application was based on choosing fibers and resin epoxies that exhibited good mechanical properties under cryogenic exposure. While there are many resin epoxies specifically for cryogenic applications, not all are commercially available. The resin Epon 828 was selected because of its properties under cryogenic conditions, ideal use for laminate infiltration and low viscosity. When combined with Epikure 3015 hardener the material system was able to cure at room temperature in 16 hours or at 93°C in only 2 hours. Woven carbon fiber and woven Kevlar fiber were selected as opposed to unidirectional fibers because of their mechanical properties in the axial and transverse direction, and the ability to resist the initiation of microcracks. The 3k plain weave carbon and plain weave Kevlar fiber material used were obtained from FIBREGLAST while the resin and hardener were both purchased from HEXION.

4.3 Manufacturing

The laminates were manufactured using the Vacuum Assisted Resin Transfer Molding (VARTM) process, which consists of two layers of flow media, four layers of peel ply and two breathers which enclosed the plain weave woven carbon and Kevlar fiber layers. The layers are placed on top of an aluminum mold and two vacuum bags enclose all the layers as seen in Fig. 22. The objective of the vacuum bags is to help infiltrate the resin and apply constant pressure during the whole curing process. The manufacturing and dimensions of the samples were based off of ASTM standards. According to the ASTM standard D7264 for standard test method for flexural properties of polymer matrix composite materials, the

samples must be 13 mm wide, 153.6 mm long, and 4 mm thick. The thickness to span length ratio must be 1:32, making the span length 128 mm. The thickness required is equivalent to 18 layers of carbon and Kevlar fibers each. Large 12"x12" laminates were assembled, as shown in Fig. 23. The resin and hardener were desiccated separately for about an hour each before infiltrating into the laminate. After curing, the samples were water jet cut to their specific sizes. Water jet cutting is a fast and effective way to cut laminates without causing delamination. Because the samples were a bit humid from the water jet cutting, they were placed in an oven to remove the extra moisture. The samples were placed in an oven at 40°C for 30 minutes, flipped over, left for another 30 min and then removed. Once all the samples were cut and dried, they were numbered and the span length was marked.

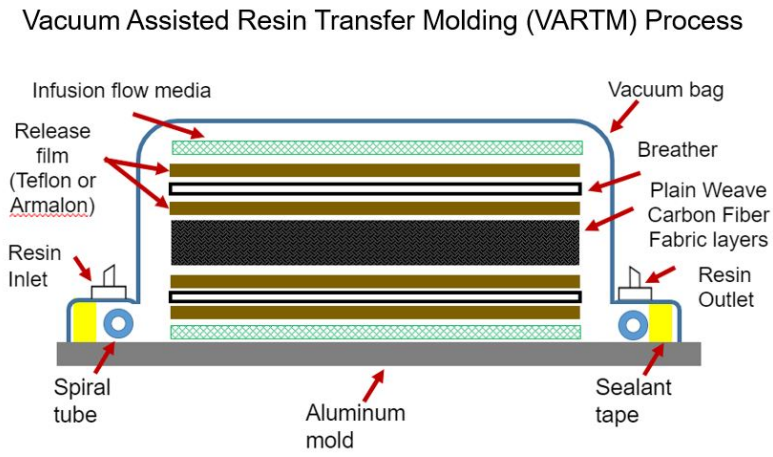

Figure 22: VARTM process illustrating layers inside vacuum bag

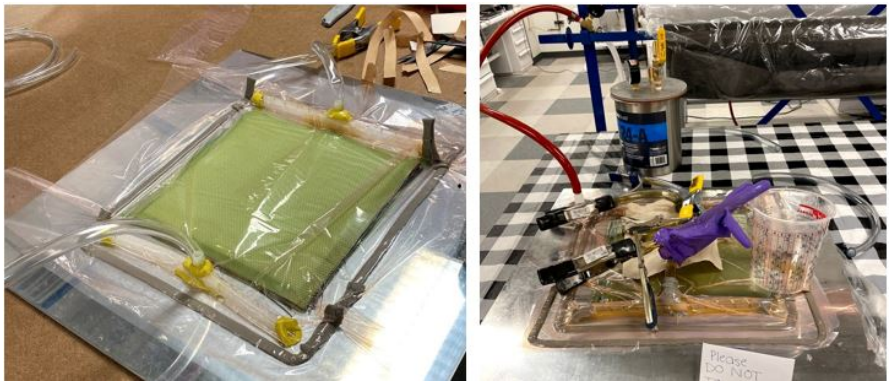

Figure 23: Laminate manufacturing using VARTM method before and after resin infusion

Figure 24: Kevlar and carbon laminates after samples were water jet cut and removed

4.4 Experiment

Testing consisted of two parts: exposing samples to corresponding temperatures, or conditioning, and a three-point bending flexural test. The samples were separated into three temperature clusters: room temperature, -60°C, and a temperature gradient of -60°C/25°C. Samples tested at -60°C were placed inside an environmental fridge for 40 hours prior to testing. Samples with a temperature gradient were conditioned using an environmental chamber. The environmental chamber exposed one surface of the sample to a -60°C environment, while keeping the opposing surface in a 25°C environment. The environmental chamber achieved this temperature gradient by being placed inside the environmental fridge at -60°C, and by having an insulated interior with a temperature-controlled heating source to maintain room temperature conditions. The samples conditioned at -60°C/25°C demonstrated that equilibrium, temperatures on either side stabilized, was reached about 40 minutes into the 5-hour conditioning time span. This created a 10° temperature gradient between both sample surfaces. Samples were removed from the environmental chamber and immediately tested. Testing was conducted in an ADMET machine with a crosshead movement rate of 1 mm/min. Each sample required a pre-load as the crosshead would not begin the tests until it was in contact with the sample. The pre-load for each sample was kept between 1 and 3 Newtons. Flexural tests were performed to obtain the maximum flexural stress and strain, flexural strength and flexural stiffness of the material system.

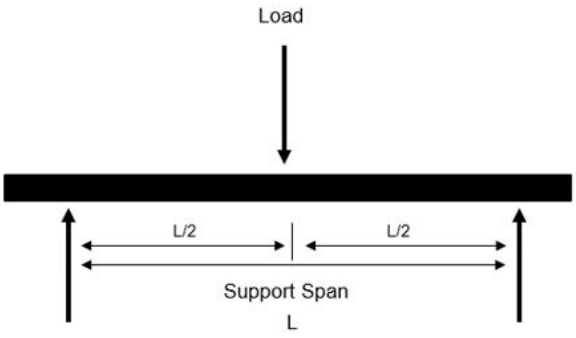

Figure 25: Flexural three-point bending test setup. The sample is placed between two supports and the load is applied at the center

4.5 Results

Flexural tests were conducted on woven carbon and woven Kevlar with Epon 828/Epikure 3015 material system. The tests were conducted after each sample was exposed to 25°C, -60°C, and a temperature gradient of 25°C/-60°C. Three-point bending tests were performed with a crosshead rate movement of 1 mm/min. The tests were performed following the ASTM D7264 standard test method for flexural properties of polymer matrix composites [15] . Contact of the crosshead with the impacted face of the sample, top surface, recorded contact force and deflection using the MTEST Quattro material testing system. The data was extracted as an excel sheet and converted into stress and strain values which were then plotted using a MATLAB code. Contact force-deflection responses display an initial linear ascending region, the slope, from which the flexural stiffness is determined. As the load increases small declines can be observed in the graph these indicate lesions in the matrix. Matrix microcracking is the first failure mode and is observed throughout the duration of the tests. The sample will fail when the fiber fractures, as can be observed in the graph when there is the sudden descend towards 0. Each sample was examined after the testing using a Q-scope digital microscope to examine the failure mechanisms. Fig. 26 and Fig. 27 show the carbon and Kevlar samples' behavior during testing.

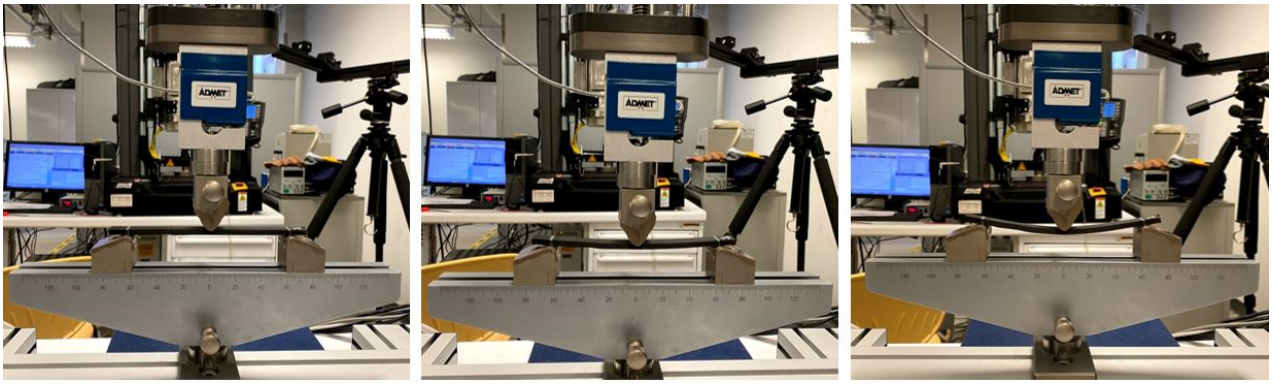

Figure 26: Carbon fiber samples during three-point bending test

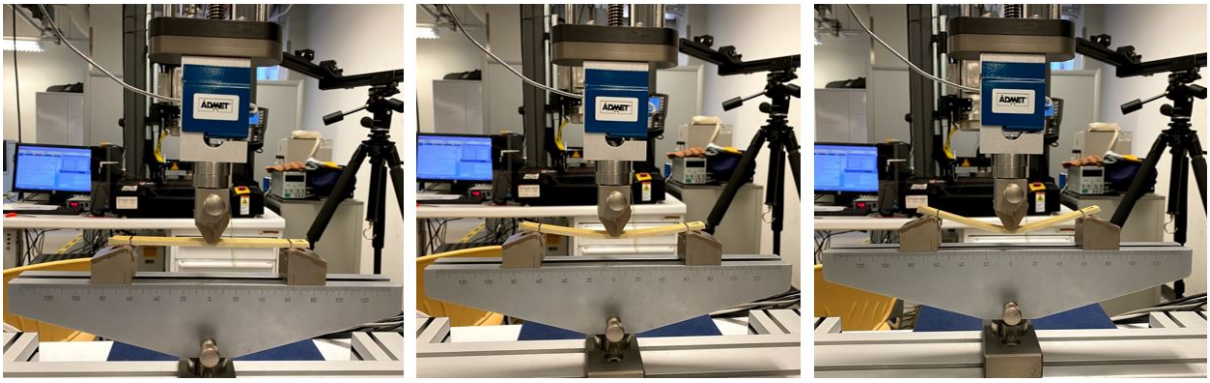

Figure 27: Kevlar fiber samples during three-point bending test

4.5.1 Carbon Fiber Samples

Room Temperature

Three carbon fiber samples were tested at room temperature. The duration of each test was about 10 minutes long and they were all able to withstand stresses above 350 MPa. All samples displayed similar behavior with signs of matrix microcracking before the fiber breakage. Samples 1 and 3 withstood stresses above 460 MPa with similar failure stresses while sample 2 only reached a failure stress of about 375 MPa, this could be due to manufacturing defects prior to testing. Sample 1 had a lower failure stress than sample 3, but had a higher fracture toughness as can be seen by the area under the curve. The main failure mechanism for these samples was fiber fracture. Fig. 29 displays sample 1 after failure. The sample's only visible failure mechanism is due to fiber fracture.

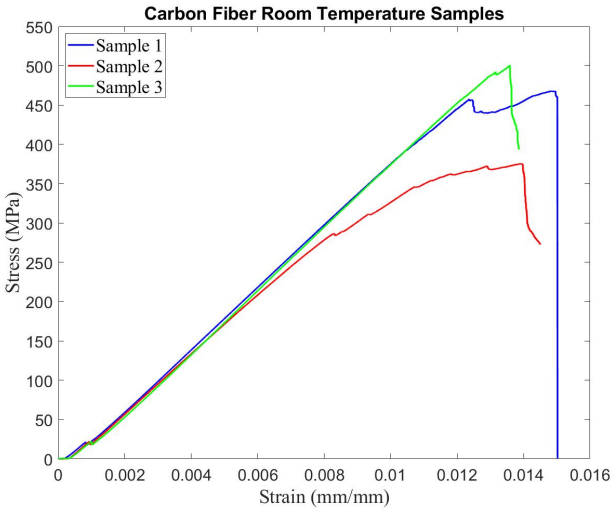

Figure 28: Stress - Strain graph of carbon fiber samples tested at room temperature

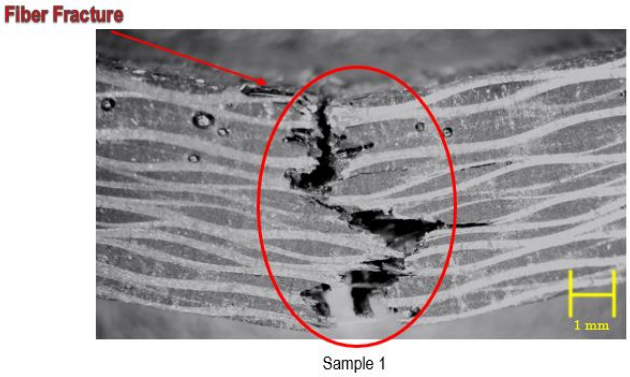

Figure 29: Microscope view of carbon fiber room temperature failure mechanism

Table 4.1: Carbon Fiber Room Temperature Samples

Sample #	Flexural Stiffness (GPa)	Ultimate Stress (MPa)	Strain at Failure
1	33.46	468.34	0.01502
2	27.81	375.87	0.01451
3	38.56	500.77	0.01387
Standard Deviation	4.39	52.92	0.00047

-60°C Temperature

Samples that were exposed to a -60°C environment had an average test duration time of 8 minutes before failing. Three samples were placed in an environmental fridge and removed individually to be immediately tested. All three samples displayed an ultimate stress above 447 MPa. The samples were able to withstand more stress than the room

temperature samples, but for less amount of time. These results are consistent because the low temperatures will increase the material toughness while making it more brittle. While there is matrix microcracking throughout the room temperature sample test, the matrix defects only occurred near failure in the low temperature samples.

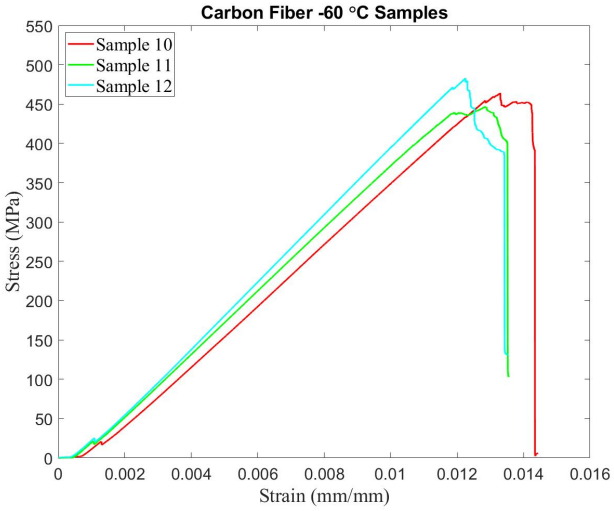

Figure 30: Stress - Strain graph of carbon fiber samples tested at -60°C

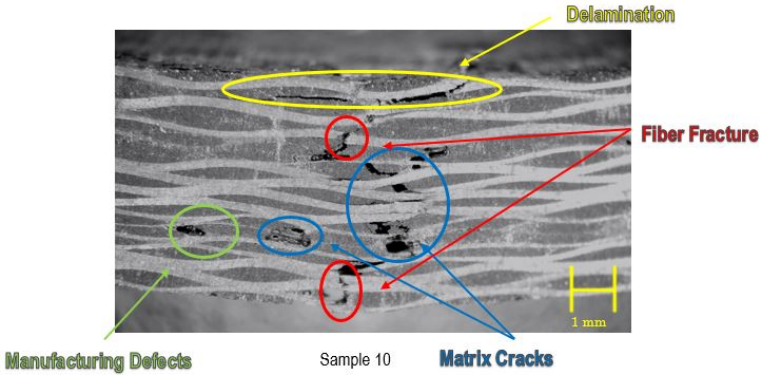

Figure 31: Microscope view of carbon fiber -60°C failure mechanism

Table 4.2: Carbon Fiber -60°C Samples

Sample #	Flexural Stiffness (GPa)	Ultimate Stress (MPa)	Strain at Failure
10	35.34	464.18	0.01434
11	36.88	447.10	0.01352
12	37.15	482.95	0.01343
Standard Deviation	0.80	14.64	0.00041

Fig. 31 above displays the failure mechanisms of sample 10. This sample displayed a wider variety of failure mechanisms when compared to the room temperature sample. Fiber delamination can be seen at the top of the sample where the force was applied. There were some visible manufacturing defects that did not directly contribute to the failure mode because they were not in the area affected by the load. Matrix cracks are distributed throughout the thickness of the sample. The woven fibers prevent matrix cracks from propagating as they are stopped by the fiber. At the very bottom of the sample there is the fiber fracture, which is expected as this part of the sample is where the most tension is experienced. This fiber fracture was not as catastrophic as the room temperature sample. That is due to the fact that sample 1 experienced an ultimate stress of 468 MPa with a strain at failure of 0.015, while sample 10 experienced an ultimate stress of 464 MPa with a strain at failure of 0.014. The fiber delamination and matrix cracks contributed to sample 10's failure.

Temperature Gradient

Samples that were exposed to the temperature gradient of (-60°C/25°C) were removed from the environmental chamber and immediately tested. The four samples had the surface exposed to -60°C as contact with the load placement. The duration of each test lasted about 9 minutes. Every sample displayed an ultimate stress higher than 455 MPa. All four samples displayed very similar behavior as they all experienced multiple matrix failures leading up to the fiber fracture. The temperature gradient sample displayed both failure mechanisms from the room temperature and -60°C samples. Again, the delamination was located near the load placement where it had been exposed to cold temperatures. Matrix cracks can be observed only towards the top surface. The fiber fracture occurred at the top surface as well. Most of the damage seemed to be on the upper surface that experienced the cold temperature exposure. Unlike the room temperature and -60°C samples, the temperature gradient sample experienced the fiber fracture in the upper surface, not at the bottom surface where the most tension is applied. The flexural stiffness and ultimate stress for these samples were very consistent, temperature gradient samples displayed the smallest standard deviation when compared to the samples entirely exposed to room temperature or -60°C environments.

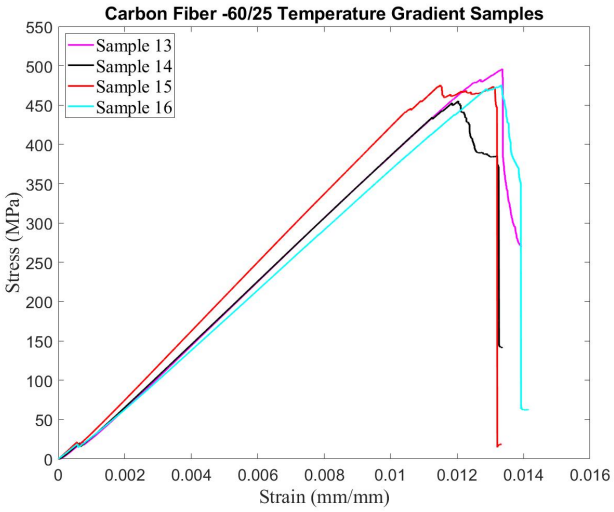

Figure 32: Stress - Strain graph of carbon fiber samples tested at -60°C/25°C

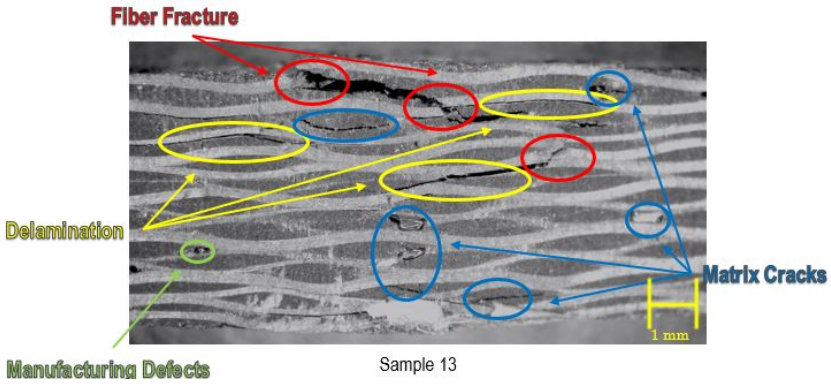

Figure 33: Microscope view of carbon fiber temperature gradient failure mechanism

Table 4.3: Carbon Fiber Temperature Gradient (-60°C/25°C) Samples

Sample #	Flexural Stiffness (GPa)	Ultimate Stress (MPa)	Strain at Failure
13	35.75	496.07	0.01394
14	34.99	455.38	0.01325
15	37.75	475.57	0.01320
16	32.85	475.72	0.01392
Standard Deviation	1.75	14.39	0.00035

4.5.2 Kevlar Fiber Samples

Room Temperature

Kevlar fiber samples tested at room temperature had an average test duration of about 17 minutes each. This was expected because of the impact absorption nature of the material.

These samples did not fail abruptly, but instead slowly began to lose strength. The samples were tested until the load being applied became constant because any further testing would only force the sample to slide between the supports without increasing the load. The ultimate stress ranged from 150 MPa through 225 MPa. The samples displayed a parabolic behavior and only showed signs of matrix microcracking after reaching their ultimate stress.

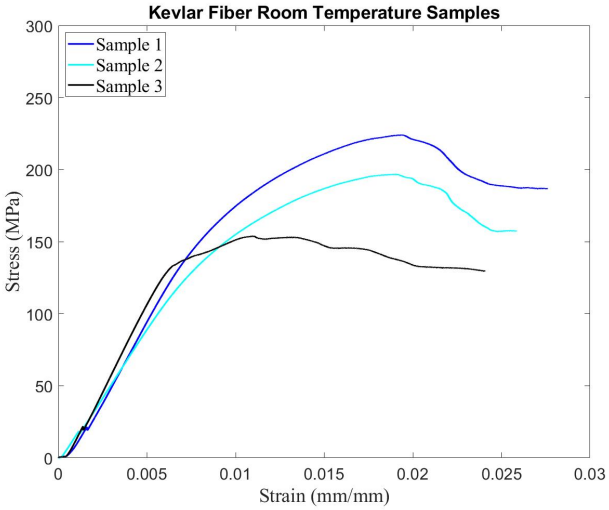

Figure 34: Stress - Strain graph of Kevlar fiber samples tested at room temperature

Figure 35: Microscope view of Kevlar fiber room temperature failure mechanism

The damage in Kevlar samples is not as clear as in carbon fiber, but Fig. 35 of sample 2 after testing displays the damage. The failure mechanism was due to delamination. All the damage occurred where the load was placed while the bottom surface does not seem to have been affected.

Table 4.4: Kevlar Fiber Room Temperature Samples

Sample #	Flexural Stiffness (GPa)	Ultimate Stress (MPa)
1	20.19	224.22
2	18.51	196.78
3	22.91	153.80
Standard Deviation	1.81	28.98

-60°C Temperature

Three samples were exposed to -60°C then tested. The average test time per sample was about 20 min. The samples were expected to fail sooner due to the brittleness, but because of the Kevlar's slow deformation rate as time went on the ice melted into the sample. Samples 11 and 12 did display a higher ultimate stress, above 235MPa, than the room temperature samples. Sample 13 followed the parabolic behavior followed by a gradual decline as well, but might have contained manufacturing defects prior to testing because of its poor performance.

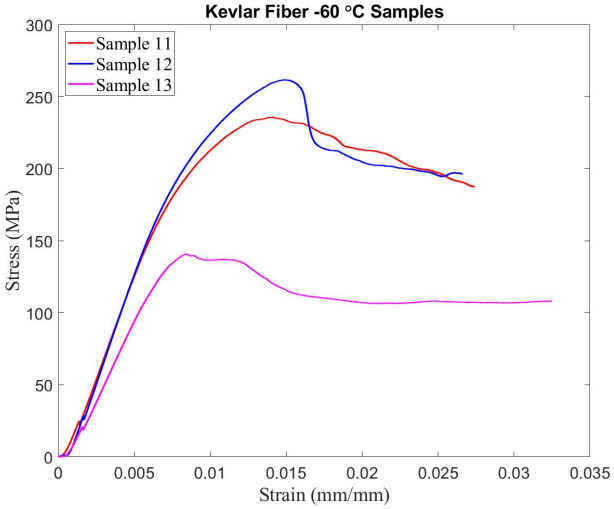

Figure 36: Stress - Strain graph of Kevlar fiber samples tested at -60°C

Table 4.5: Kevlar Fiber -60°C Samples

Sample #	Flexural Stiffness (GPa)	Ultimate Stress (MPa)
11	11.43	235.88
12	27.63	261.82
13	20.48	140.73
Standard Deviation	6.63	52.06

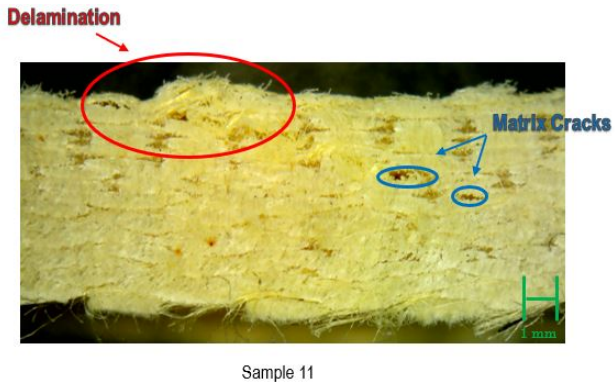

Figure 37: Microscope view of Kevlar fiber -60°C failure mechanism

Under a -60°C environment the samples did not fail abruptly, but in some the loss of strength was more apparent. The failure mechanism of sample 11 is a combination of delamination and matrix cracks. The delamination is located where the load was applied, but the matrix cracks appear too distant from the area where the load was applied. The matrix cracks may not have contributed to the failure of this specific sample, but were created due to the exposure to low temperatures.

Temperature Gradient

Four samples were exposed to a temperature gradient of -60°C/25°C. The load was applied on the surface exposed to -60°C. All samples began following a parabolic pattern, but samples 14 and 17 failed abruptly instead of steadily declining. An abrupt failure in the graph means fiber fracture, by inspecting sample 14 it is not apparent where the fracture occurred, but it can be seen that there is delamination where the load was applied.

Table 4.6: Kevlar Fiber Temperature Gradient (-60°C/25°C) Samples

Sample #	Flexural Stiffness (GPa)	Ultimate Stress (MPa)
14	27.57	242.04
15	27.79	249.96
16	27.95	252.65
17	26.96	257.08
Standard Deviation	0.38	5.47

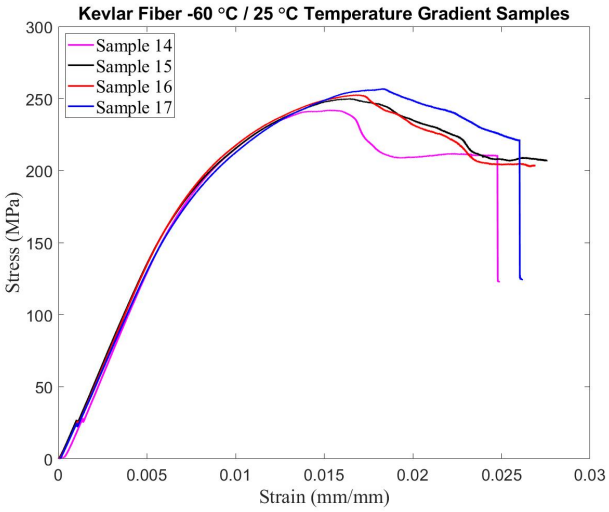

Figure 38: Stress - Strain graph of Kevlar fiber samples tested with -60°C / 25°C temperature gradient

Figure 39: Microscope view of Kevlar fiber -60°C / 25°C temperature gradient failure mechanism

4.6 Conclusions

The exposure of plain-woven carbon fiber and plain-woven Kevlar fiber with Epon 828/ Epikure 3015 to different environments has an effect on their failure mechanisms. The flexural stiffness and ultimate strength of carbon and Kevlar fibers fluctuated when exposed to different temperatures, but coincided with what was expected based on their material properties. While the fiber properties were not significantly affected by the different environments, the matrix system was. The goal of this study was to concentrate on not when the sample will fail, but how it would fail by studying their failure mechanism. Both carbon and Kevlar

temperature gradient samples displayed both failure mechanisms for room temperature and -60°C exposure. In carbon fiber, failure modes were very clear, delamination and matrix microcracking occurred in both surfaces that had been exposed to cold temperatures. Kevlar samples however were not as clear to examine. Delamination was present anywhere the load was applied, but fiber fracture was not visible. Carbon fiber samples were able to withstand a larger amount of stress when compared to Kevlar, but for a much smaller amount of time. The Kevlar samples were able to handle larger amounts strain at smaller loads. With the use of woven fibers, matrix cracks were present as expected, but were unable to propagate throughout the sample. Instead of one matrix crack propagating along the whole sample, small and spread out matrix cracks were present. Material properties obtained from this study can be applied in simulations to test the use of these materials in cryogenic propellant tank applications. Understanding the properties and failure mechanisms of this material system can lead to an optimized fiber layup to create an all composite propellant tank.

Chapter 5

Matrix System

5.1 Introduction

The selection of a resin material system for a cryogenic linerless all composite tank can have a monumental impact on its success. When exposed to cold temperatures resin becomes brittle and is subject to microcracking. Many material systems, fiber and matrix, are tested to obtain their mechanical properties under certain environmental conditions. In this study the mechanical properties of the matrix system, Epon 828 resin and Epikure 3015 hardener, are obtained by testing samples at room temperature and after exposure to a -60°C environment.

5.2 Manufacturing

The material system for the matrix consisted of Epon 828 resin and Epikure 3015 hardener, both purchased from HEXION. The resin data sheet specified that when hardened with an appropriate curing agent, very good mechanical, adhesive, dielectric and chemical resistance properties would be obtained. The recommended concentration from the manufacturer's data sheet was a 100:50 ratio by weight of resin to hardener. The manufacturer also stated that the matrix would cure at room temperature after 16 hours, and in only two hours at 93°C. The resin was clear and semi viscous, while the hardener an orange color with a much more viscous consistency. Both products were poured and weighed in separate containers, then mixed together. The mixture was stirred until a uniform cream color could be seen. The resulting mix was very thick and many air bubbles were present. The sample size was determined using the ASTM D790-17 Standard Test Methods for Flexural Properties of Unreinforced and Reinforced Plastics and Electrical Insulating Materials. Sample sizes must follow a 16:1 span length to thickness ratio. Samples 3.2 mm or less in thickness must have a width of 12 mm and the overhang on either side of the support span must be at least 10% of the support span length, but never less than 6.4 mm. The samples had a thickness of 3.2 mm, a support span of 51.2 mm, and an overall length of 64 mm [16]. In order to achieve these sample dimensions, cast resin molds were 3D printed. Two different manufacturing methods were used to produce resin samples.

Figure 40: 3D printed cast resin molds for sample manufacturing

5.2.1 Method 1

The amount of resin and hardener needed to produce these samples was so small the mixture was desiccated together; this process was not very successful in removing air bubbles. When used in larger quantities, it was more efficient to desiccate resin and hardener separately. The resin and hardener were then desiccated separately and after removing the majority of the air bubbles, the resin mixture was poured into the molds. The molds were left to cure at room temperature conditions for 16 hours. After the sample was removed from the mold, air bubbles could still be seen inside the sample giving it a very opaque appearance with yellowish color. The presence of air bubbles in the sample are considered manufacturing defects; which can affect the sample's performance during testing.

5.2.2 Method 2

A second approach at manufacturing the resin samples was attempted. As proven by the last batch of samples, very small air bubbles were unable to be removed from the mixture with the desiccator. The new approach consisted of mixing the resin and hardener and placing the mixture in the molds without desiccating. The molds were then placed in an oven for two and a half hours at 95°C. This process was very successful in removing air bubbles within the sample. The new samples had little to none visible air bubbles and the sample had a clear see through appearance. Fig. 42 compares the two manufacturing method results.

Figure 41: Method 1 resin sample with visible air bubbles on its surface

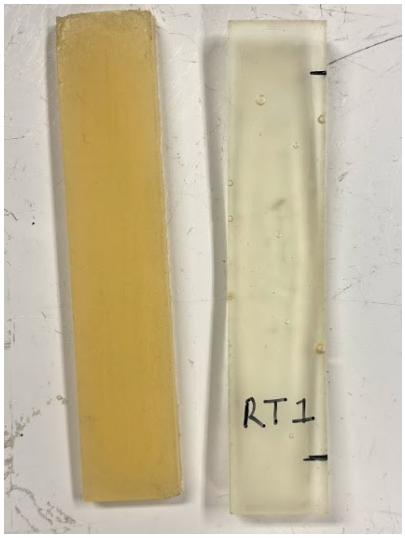

Figure 42: Sample comparison of Method 1 sample (left) and Method 2 sample (right). Method 2 sample shows little to none air bubbles.

5.3 Testing

A three-point bending test was performed to obtain the flexural properties of the matrix material system. Prior to testing, each sample was labeled and its dimensions were measured and recorded. The samples were tested using the ADMET 500 lbf machine with 5 mm supports and a crosshead rate of 1 mm/min. Contact of the crosshead with the impacted face of the sample recorded contact force and deflection using the MTEST Quattro system.

The data was extracted as an excel sheet and converted into stress and strain values which were then plotted using a MATLAB code. The samples were tested at 25°C and -60°C. To condition the low temperature samples, they were placed inside an environmental fridge at -60°C for 40 hours prior to testing. Testing of each individual sample stopped once it exceeded its 5% strain limit. The deflection at which this strain would occur was calculated using equation 2 of the ASTM790, as show below.

$$D = \frac{rL^2}{6d} \tag{5.1}$$

Where D is the midspan deflection, r is the strain limit (0.05 in this case), L is the support span, and d is the depth of beam. The deflection at which the sample reached its 5% strain was calculated to be 6.8 mm.

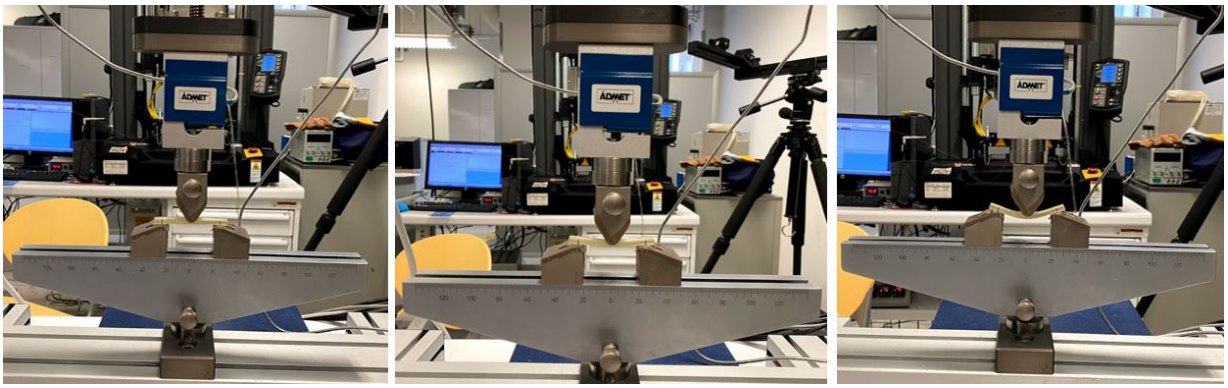

Figure 43: Flexural testing of the resin samples

25°C Samples

Five samples were tested at 25°C and had an average time of 8 minutes each before they reached a 5% strain limit. The samples displayed a considerable amount of deformation after undergoing flexural testing, but slowly returned to their original shape. This is a great sign of the plastic properties of the matrix material system. The flexural stiffness was obtained from the plastic region of the samples, in this case it was up until the 0.02 strain where a linear behavior was observed. The samples had an average flexural stiffness of 3.09 GPa and all samples were able to withstand an ultimate stress greater than 88 MPa. All samples reached their strain limit before failure.

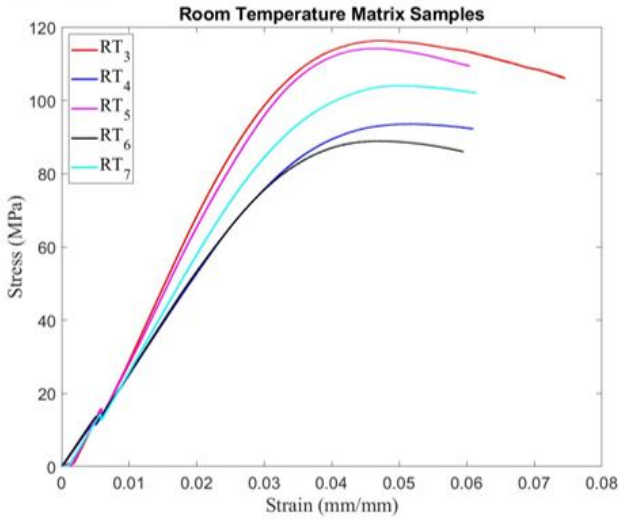

Figure 44: Stress - Strain graph results of resin room temperature samples

Table 5.7: Room Temperature Matrix Samples

Sample	Flexural Stiffness (GPa)	Ultimate Stress (MPa)
RT3	3.62	116.46
RT4	2.66	93.66
RT5	3.46	114.24
RT6	2.67	88.95
RT7	3.02	104.15
Standard Deviation	0.40	10.88

-60°C Samples

Five samples were tested at -60°C. The samples were removed from the environmental fridge individually and immediately placed for testing. The average time for each test was about 8 minutes before the sample reached the 5% strain limit. Linear behavior was only observed up to a 0.005 strain. The average flexural stiffness for the samples was 1.65 GPa and they were all able to withstand an ultimate stress greater than 38 MPa. The flexural stiffness of the matrix system decreased by about half when exposed to cold temperatures.

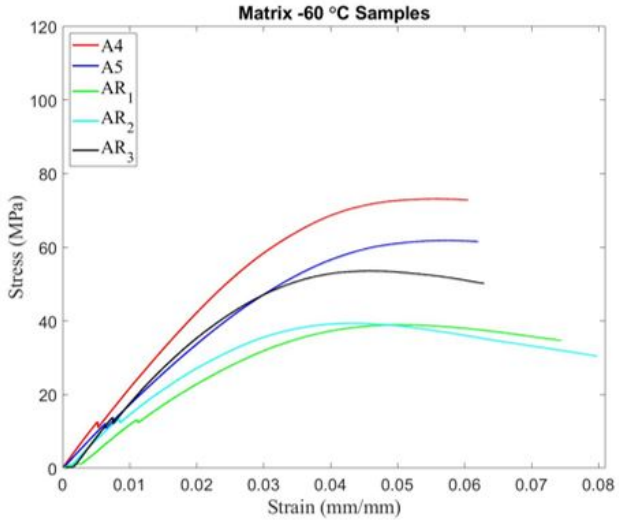

Figure 45: Stress - Strain graph results of resin -60°C samples

Table 5.8: -60°C Matrix Samples

Sample	Flexural Stiffness (GPa)	Ultimate Stress (MPa)
A4	2.09	73.19
A5	1.67	61.91
AR1	1.22	38.99
AR2	1.39	39.39
AR3	1.89	53.60
Standard Deviation	0.32	13.18

5.4 Conclusion

The decrease in flexural stiffness was expected due to cold temperatures having a brittle effect on the matrix samples. The variation within the room temperature and cold samples could have been affected by the sample manufacturing. The system displayed good material properties even under the cold environment. There was no indication of matrix microcracking before reaching the strain limit. Multiple batches of resin samples were manufactured in order to have enough samples for testing. Because of the high resin to hardener ratio and the small quantity needed for matrix samples, any small imbalance in measurement could have an impact in the sample properties. Future testing will be conducted by only using samples from the same manufactured batch.

Chapter 6

Centennial Small Payload Launch Vehicle Second Stage Composite Common-Bulkhead Tank

6.1 Introduction

Generally when small payloads are to be launched, they must wait to be integrated into the launch of a larger vehicle which may take months. They are not taken as the primary payload and may be damaged before even making it into their orbit. Creating a launch vehicle specifically for small payloads will allow to have faster, safer, and cheaper launches into orbit. Additive manufacturing is a great new tool for the aerospace industry because it allows for the use of composite materials with lighter and stronger properties. The Center for Space Exploration and Technology Research (cSETR) is designing an innovative launch vehicle that will carry a small payload into low earth orbit (LEO). The goal is to reduce launch cost by introducing innovative designs into the vehicle. In order to attempt and minimize any possible errors, the design will be as simple as possible. This will be possible due to innovations like common-bulkhead tanks, a pressure fed system, LOX Methane engines and carbon composite materials. In most launch vehicles the use of a pump fed system is common; this system uses turbopumps to feed propellant into the engine. Replacing this system for a pressure fed system removes the use for turbo pumps and increases reliability. Turbomachinery can be complicated, expensive, and heavy. Using an ablative pressure fed approach reduces complexity of the system and the number of potential failures [17]. Pressure fed systems use a constant feed of high pressurant gas to displace liquid propellant in the fuel and oxidizer tanks into the engine. Due to the high pressurization needed, pressure fed tanks tend to be thicker than the thin pump fed low pressure ones. Launch vehicles with simple pressure fed propulsion systems have been attempted in the past, but usually result in very high dry mass fractions. Replacing traditional metal alloy tanks with carbon composite ones can minimize their weight. The focus of this paper will be on the design of the second stage tank of the vehicle.

6.2 Tank Calculations

To begin, the size and inert mass fraction were calculated for the overall launch vehicle. This was based off the isp for the propellant, payload, and distance to the desired orbit. Some parameters were given for the design of the small payload vehicle, that included the use of UTEP's CROME engine: which runs using LOX/Methane, a 100 lb payload, and a low earth orbit (LEO) goal. Using the given parameters, it was determined a two and a half stage vehicle using boosters would make this possible. This study concentrates only on the second stage tank design and calculations. All calculations were done on MATHCAD to avoid mathematical and unit conversion errors. Table 6.9 below shows the main properties and parameters used.

Table 6.9: Tank Properties

Fuel Density	422.62 (gm/L)
Oxidizer Density	1.141 (gm/cm^3)
Helium Pressure	2000 psi
Fuel Pressure	400 psi
Oxidizer Pressure	400 psi
Propellant Mass	1171 lb
Oxidizer/Fuel Ratio	2.7

Table's 6.9 properties determined the volumes and size dimensions for the second stage common bulkhead tank. Appendix A shows the steps and equations to find the tank dimensions. This includes fuel and oxidizer volumes, tank diameters and lengths. In order to create a common-bulkhead tank, the helium, or uppermost tank's diameter was used as a reference point for the rest of the tank. The diameter for the helium was based off two factors: the overall diameter of the whole vehicle, it could tapper in or out and change the L/D of the vehicle; and on the pressure, the smaller the tank the higher the pressure. Because of the helium tank's high pressure, it was designed to be a spherical tank. To create the bulkhead portions a cylindrical section was attached to the helium tank. This means the fuel and oxidizer tanks each need a cylindrical and spherical section. In order to feed the CROME engine the fuel and oxidizer tanks had to maintain a pressure of 400 psi.

6.3 Tank Thickness

In order to define the thickness for each portion of the common-bulkhead tank, thin pressure vessel equations were utilized. Since the pressure vessel consists of cylindrical and spherical sections the tank is not one uniform thickness.

$$\sigma_{cylinder} = \frac{PD}{2t} \tag{6.2}$$

The hoop stress equation above was used for the cylindrical sections of the oxidizer and fuel tank. P is the internal pressure of the vessel, D is the diameter and t is the thickness. For the spherical sections, longitudinal stress equation was used.

$$\sigma_{sphere} = \frac{PD}{4t} \tag{6.3}$$

The equations for each were rearranged to solve for thickness:

$$t = \frac{PD}{2\sigma_{cylinder}} \tag{6.4}$$

$$t = \frac{PD}{4\sigma_{sphere}} \tag{6.5}$$

Safety factors are also an important design aspect to consider. According to the ASME Boiler and Pressure Vessel Code metallic pressure vessels have a safety factor requirement of 2.5. Composite materials have a much higher safety factor which ranges from 3.5 to 6.

6.4 Material and Weight

The next step was to choose the tank material. To reduce the overall weight of the tank, composite materials will be used. When manufacturing composite tanks, it is really important to choose the right material system. Composite tanks have generally been manufactured using unidirectional fibers. The strength is large in the axial, or along the fiber direction, but when exposed to transverse stresses the composite only depends on the matrix. This results in a very large thickness for the tank. Using woven fibers on the other hand gives the material system the same properties in all directions so when stress is applied matrix and fiber are both affected. This greatly reduces the thickness of the tank. Another important

factor is manufacturing methods. The manufacturing of composites can have a great impact on its mechanical properties as pressure and temperatures can vary. Autoclave and VARTM methods result in different fiber volume fractions, the higher the volume fraction the more compacted the fibers are, and the better the material properties. Table 6.10 below compares different material systems mechanical properties and how they compare on the overall weight of the tank. The values and dimensions used were from tank dimensions and tank thickness calculations from appendix B-E. When using a safety factor of 6, thin wall pressure vessel equations will not be viable for the helium tank due to its high pressure and wall thickness. In order to meet the thin wall pressure vessel requirements, the inner radius divided by its thickness must be greater than or equal to 10.

Table 6.10: Material System Comparison

Material System	F.O.S	M.O.S	Fiber Volume Fraction	Total Weight (kg)
CF/EPON 828/EPIKURE 3015 (-60°C)	3.5	1.5	0.45-0.5	248.247
	6	1.5	0.45-0.5	425.567
CF/EPON 828/EPIKURE 3015 (25°C)	3.5	1.5	0.45-0.5	257.338
	6	1.5	0.45-0.5	441.152
CF/EPON 828/EPIKURE 3015 (25°C/-60°C)	3.5	1.5	0.45-0.5	242.537
	6	1.5	0.45-0.5	415.779
AS4/3501-6 (Axial)	3.5	1.5	0.62	51.288
	6	1.5	0.62	87.922
AS4/3501-6 (Transverse)	3.5	1.5	0.62	2052.474
	6	1.5	0.62	3518.527
Al 2219 T87	2.5	1.5	-	307.297

Table 6.10 compares two composite material systems with a metallic alloy using different factors to calculate the tank weight. The two composite material systems compared are woven carbon fiber with epon 828/epikure 3015 hardener and AS4 with 3501-6. The woven carbon fiber with Epon 828/Epikure 3015 system includes the properties from the material being tested at room temperature, -60°C and a (-60°C/25°C) temperature gradient. The system was manufactured using the VARTM method resulting in a 0.45 to 0.5 fiber volume fraction. Because its is a composite it is also calculated for a safety factor of 3.5 and then for a safety factor of 6. Although the properties did have an impact on the weight, they were all very similar and had an average of 249 kg for a safety factor of 3, and an average of

427 kg for a safety factor of 6. For the AS4/3501-6 material system the properties are only from room temperature conditions. This is a unidirectional fiber and so both the axial and transverse properties are calculated at 3.5 and 6 safety factors. This system has a higher fiber volume fraction at 0.62. It displayed very good properties in the axial direction making the tank less than 100 kg, but in the transverse direction the weight exponentially grows to above 2000 kg. Finally, metal alloy Al 2219 T87 is compared with a safety factor of 2.5 and has a weight of 307 kg. The material systems are also compared using a strength vs stiffness graph as shown below.

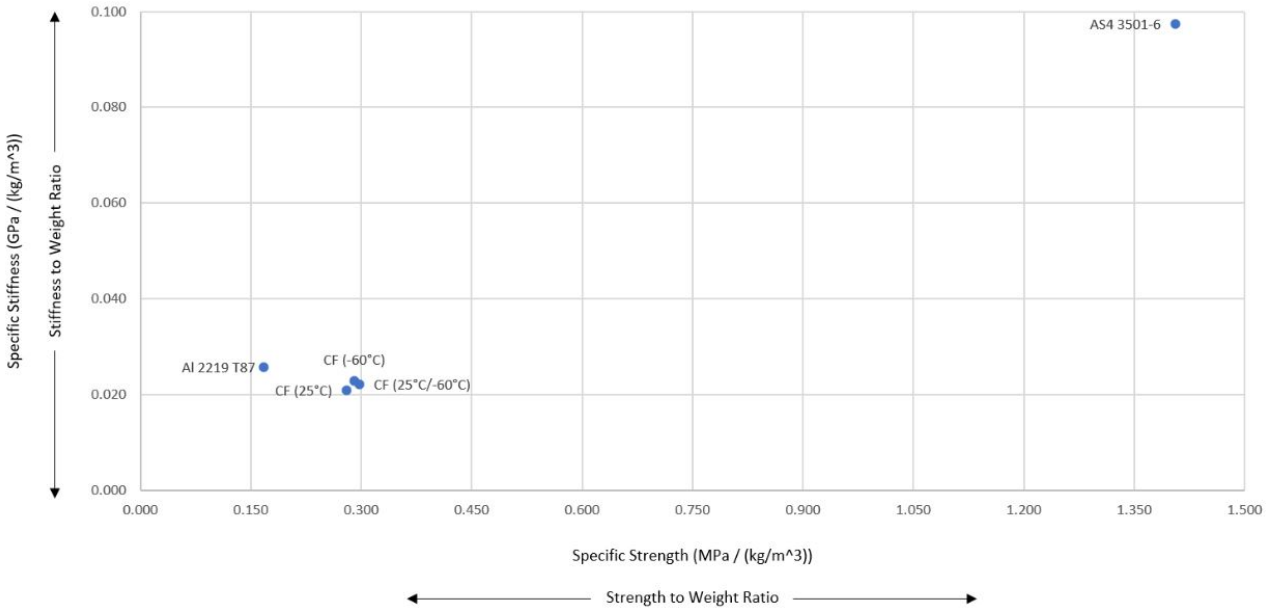

Figure 46: Strength vs Stiffness graph compares three different material systems

The strength-stiffness graph indicates where carbon fiber Epon 828/Epikure 3015 stands compared with other commonly used material systems for pressure vessels. The system behaves similarly for all its different environmental exposures as they are all clustered together. This material system has a better strength to weight ratio than common Al 2219 T87 and is very close to matching its stiffness-to-weight ratio. AS4 3501-6 has a very good strength-to-weight and stiffness-to-weight ratio. This composite is far better than using an aluminum alloy. When compared to our carbon fiber Epon 828/Epikure 3015 it is also better. One of the considerations for this project was finding a commercially available material system. Although AS4 3501-6 is commercially available, its cost is also very high. The price for a whole gallon epoxy for our system is the price for only a quarter of the AS4 3501-6.

6.5 CAD Model

The CAD models were all done using Siemens NX 11 software. The model was designed in three different sections to resemble the assembly process of the tanks. The helium tank is spherical and defined the overall diameter of the common-bulkhead vessel. The oxidizer and fuel tanks are very similar, the only difference is slight changes in length. The parts will fit into each other as they are manufactured and assembled together. The following figures show the individual tanks and the complete assembly.

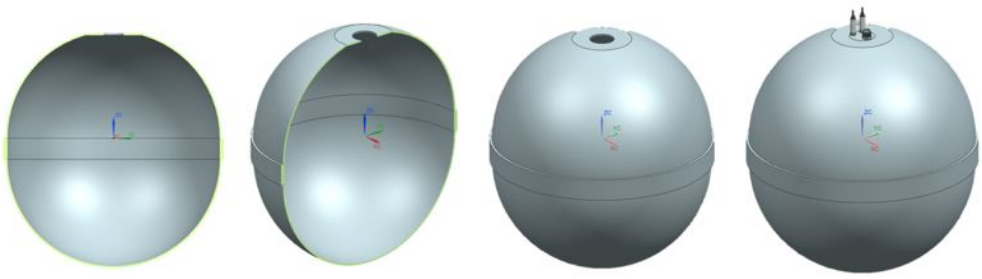

Figure 47: Helium Tank

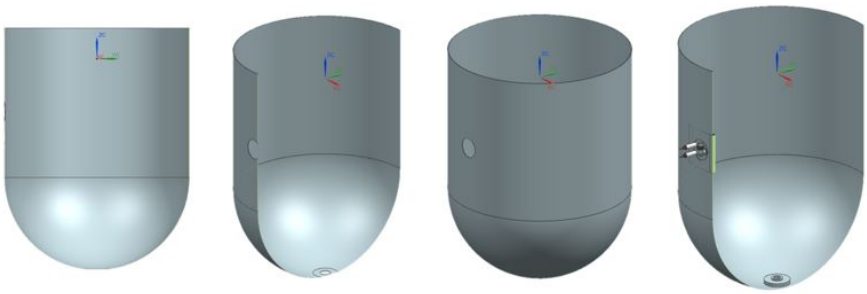

Figure 48: Fuel Tank

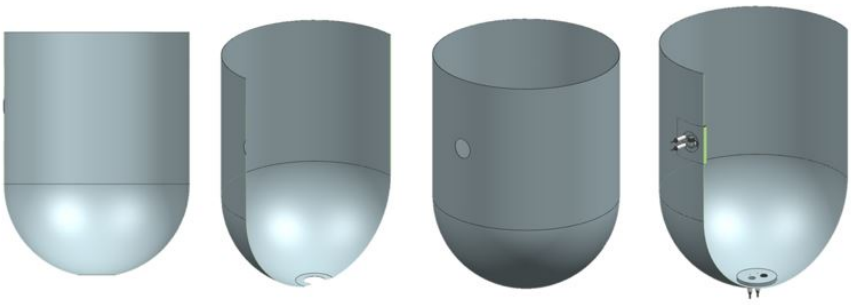

Figure 49: Oxidizer Tank

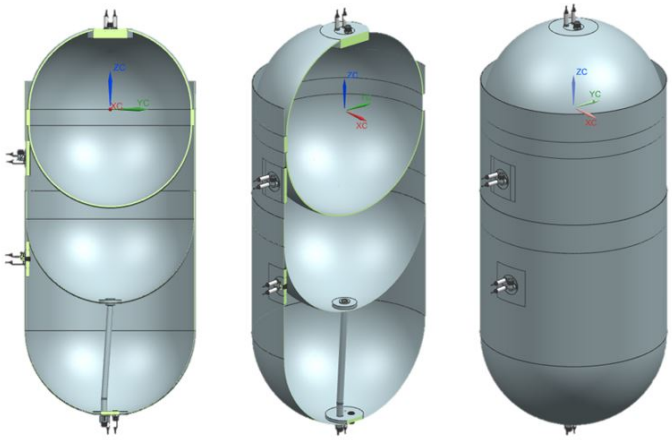

Figure 50: Complete assembly of commonbulkhead tank

6.6 Conclusion

The commercially available material system of woven carbon fiber with epon 828/ epikure 3015 is a viable option for the manufacturing of a cryogenic common-bulkhead tank in launch vehicle applications. Its mechanical properties were tested under three different environments: room temperature, -60°C, and with a temperature gradient of (25°C/-60°C). When compared to unidirectional fiber material system the weight savings are about 8 times less in weight. When compared to a traditional metal alloy tank the weight savings are about 58 kg when using a 3.5 safety factor.

References

[1] John Cronin, Kaushik Mallick, Mark Lake, and Naseem Warner Munshi. Damage and leakage barrier in all composites pressure vessel and storage tanks. 2:14, 2008.

[2] D. M. Ó Grogan, C. M. Brádaigh, J. P. McGarry, and S. B. Leen. Damage and permeability in tape-laid thermoplastic composite cryogenic tanks. *Composites Part A: Applied Science and Manufacturing*, 78:390–402, 2015.

[3] Md.S. Islam, E. Melendez-Soto, A.G. Castellanos, and P. Prabhakar. Investigation of woven composites as potential cryogenic tank materials. *Cryogenics*, 72:82–89, 2015.

[4] Kaushik Mallick, John Cronin, Steven Arzberger, Lorie Tupper, Michael L.and Grimes-Ledesma, Joseph C. Lewis, Chris Paul, and Jeffry S. Welsh. Ultralight linerless composite tanks for in-space applications. *A Collection of Technical Papers - AIAA Space 2004 Conference and Exposition*, 1:1–13, 2004.

[5] Hong Wei He and Feng Gao. Effect of fiber volume fraction on the flexural properties of unidirectional carbon fiber/epoxy composites. *International Journal of Polymer Analysis and Characterization*, 20:180–189, 2015.

[6] William James Clark and Robert John Wetherall. Common bulkhead cryogenic propellant tank. 1, 2002.

[7] Hei Lam Ma, Zhemin Jia, Kin Tak Lau, Jinsong Leng, and David Hui. Impact properties of glass fiber/epoxy composites at cryogenic environment. *Composites Part B:Engineering*, 92:210–217, 2016.

[8] S. Sánchez-Sáez, T. Gómez-Del Río, E. Barbero, R. Zaera, and C. Navarro. Static behavior of cfrps at low temperatures. *Composites Part B:Engineering*, 33:383–390, 2002.

[9] B. V. Sunil Kumar, Neelakantha V. Londe, A. O. Surendranathan, and K. Anilas. Study on mechanical cryogenic properties of carbon epoxy composites. *IOP Conference Series: Materials Science and Engineering*, 376, 2018.

[10] S. P. Zaoutsos and M. C. Zilidou. Influence of extreme low temperature conditions on the dynamic mechanical properties of carbon fiber reinforced polymers. *IOP Conference Series: Materials Science and Engineering*, 276, 2017.

[11] Takahira Aoki, Hisashi Kumazawa, Takashi Ishikawa, and Yoshiki Morino. Mechanical behavior of cf/polymer composite laminates under cryogenic environment. *41st Structures, Structural Dynamics, and Materials Conference and Exhibit*, 04 2000.

[12] F.C. Campbell. Introduction to composite materials. pages 1–18, 2010.

[13] HEXION. Epon resin 828 technical data sheet. *https://www.hexion.com/en-US/product/epon-resin-828*, pages 98–99, accessed March 15, 2020.

[14] Theodore F. Johnson, David W. Sleight, and Robert A. Martin. Structures and design phase i summary for the nasa composite cryotank technology demonstration project. *54th AIAA/ASME/ASCE/AHS/ASC Structures, Structural Dynamics, and Materials Conference*, pages 1–11, 2011.

[15] ASTM International. D7264/d7264m: Standard test method for flexural properties of polymer matrix composite materials. *Annual Book of ASTM Standards*, i:1–11, 2015.

[16] ASTM International. D790-03-standard test method for flexural properties of unreinforced and reinforced plastics and electrical insulation materials. *Annual Book of ASTM Standards*, pages 1–11, 2015.

[17] Dr. Shyama Chakroborty Bauer and Dr. Thomas P. Using pressure-fed propulsion technology to lower space transportation costs. *40th AIAA/ASME/SAE/ASEE Joint Propulsion Conference and Exhibit*, pages 1–9, 2004.

Appendix A

Commonbulkhead Tank Volume and Overall Dimensions

Commonbulkhead Tank Volume and Sizes

Second Stage

All variables needed to solve for tank weight and sizes

$\rho_{fuel} := 422.62 \ \frac{gm}{L}$ $\rho_{ox} := 1.141 \ \frac{gm}{cm^3}$

$m_{prop} := 1171 \ lb$ (Total propellant mass needed)

$P := 400 \ psi$ (Pressure of one individual fuel or oxidizer tank)

$P_H := 2000 \ psi$

$f_s := 2.7$ (Oxidizer/Fuel ratio)

Find the weight and volume of fuel and oxidizer tank

$m_{fuel} := \frac{m_{prop}}{1 + f_s} = 316 \ lb$ $V_{fuel} := \frac{m_{fuel}}{\rho_{fuel}} = 12 \ ft^3$

$m_{ox} := m_{prop} \cdot \frac{f_s}{f_s + 1} = 855 \ lb$ $V_{ox} := \frac{m_{ox}}{\rho_{ox}} = 12 \ ft^3$

Add ullage, boiling, and trapped volume to get the final volume of each tank

$V_{ull} := 0.03$ $V_{boil} := 0.03$ $V_{trap} := 0.05$

$Vt_{ox} := V_{ox} + V_{ox} \cdot V_{ull} + V_{ox} \cdot V_{boil} + V_{ox} \cdot V_{trap} = 13 \ ft^3$

$Vt_{fuel} := V_{fuel} + V_{fuel} \cdot V_{ull} + V_{fuel} \cdot V_{boil} + V_{fuel} \cdot V_{trap} = 13 \ ft^3$

Find mass of helium needed to feed propellant tanks

$R_H := 12420 \ \frac{ft \cdot lbf}{R \cdot slug}$

$T := 162.27 \ R$ (Temperature of oxygen at cryogenic temperatures)

$m_H := \frac{P \cdot (Vt_{ox} + Vt_{fuel})}{R_H \cdot T} = 24.488 \ lb$

Now find Volume of Helium tank needed to keep two propellant tanks pressurized

$$V_H := \frac{2 \cdot m_H \cdot R_H \cdot T}{P_H} = 10.653\ ft^3 \qquad m_H := m_H + \frac{P \cdot (V_H)}{R_H \cdot T} = 34.284\ lb$$

$$V_H := \frac{2 \cdot m_H \cdot R_H \cdot T}{P_H} = 14.914\ ft^3$$

Solve for the size dimensions of helium, oxidizer, and fuel

Helium tank diameter sets the overall dimensions for the rest of the tanks

$$Di := 35\ in \qquad r := \frac{Di}{2}$$

Find cylindrical length of oxidizer tank

$$L_{ox} := \frac{Vt_{ox}}{\pi \cdot r^2} = 23.916\ in$$

Find cylindrical length of fuel tank

$$L_{fuel} := \frac{Vt_{fuel}}{\pi \cdot r^2} = 23.91\ in$$

Appendix B

Woven CF/EPON 828/EPIKURE 3015

Helium Tank (Spherical)

-60°C Carbon Fiber

Pressure (MPa)	M.O.S	M.O.S Pressure (MPa)	Radius (m)	F.O.S	σ (UTS) (MPa)	σ (allow) (MPa)	t (mm)	Surface Area (mm^2)	Density (g/mm^3)	Weight (kg)	Thin Wall (r/t)>10
13.789	1.5	20.684	0.4445	3.5	464.180	132.623	34.661	2482866.648	0.0016	137.696	12.824
13.789	1.5	20.684	0.4445	3.5	447.096	127.742	35.986	2482866.648	0.0016	142.957	12.352
13.789	1.5	20.684	0.4445	3.5	482.946	137.985	33.315	2482866.648	0.0016	132.345	13.342
13.789	1.5	20.684	0.4445	3.5	464.741	132.783	34.620	2482866.648	0.0016	137.530	12.840
13.789	1.5	20.684	0.4445	6	464.741	77.457	59.348	2482866.648	0.0016	235.765	7.490
Room Temperature Carbon Fiber (25°C)											
13.789	1.5	20.684	0.4445	3.5	468.335	133.810	34.354	2482866.648	0.0016	136.474	12.939
13.789	1.5	20.684	0.4445	3.5	375.868	107.391	42.805	2482866.648	0.0016	170.048	10.384
13.789	1.5	20.684	0.4445	3.5	500.765	143.076	32.129	2482866.648	0.0016	127.636	13.835
13.789	1.5	20.684	0.4445	3.5	448.323	128.092	35.887	2482866.648	0.0016	142.566	12.386
13.789	1.5	20.684	0.4445	6	448.323	74.720	61.521	2482866.648	0.0016	244.399	7.225
Temperature Gradient (-60°C / 25°C)											
13.789	1.5	20.684	0.4445	3.5	496.067	141.733	32.433	2482866.648	0.0016	128.845	13.705
13.789	1.5	20.684	0.4445	3.5	455.376	130.107	35.332	2482866.648	0.0016	140.358	12.581
13.789	1.5	20.684	0.4445	3.5	475.566	135.876	33.832	2482866.648	0.0016	134.399	13.139
13.789	1.5	20.684	0.4445	3.5	475.718	135.919	33.821	2482866.648	0.0016	134.356	13.143
13.789	1.5	20.684	0.4445	3.5	475.682	135.909	33.823	2482866.648	0.0016	134.366	13.142
13.789	1.5	20.684	0.4445	6	475.682	79.280	57.983	2482866.648	0.0016	230.342	7.666

Fuel Tank (Cylindrical)

-60°C Carbon Fiber

Pressure (MPa)	M.O.S	M.O.S Pressure (MPa)	Radius (m)	F.O.S	σ (UTS) (MPa)	σ (allow) (MPa)	t (mm)	Surface Area (mm^2)	Density (g/mm^3)	Weight (kg)	Thin Wall (r/t)>10
2.757	1.5	4.1355	0.461518	3.5	464.180	132.623	14.391	1692591.881	0.0016	38.974	32.069
2.757	1.5	4.1355	0.461518	3.5	447.096	127.742	14.941	1692591.881	0.0016	40.463	30.889
2.757	1.5	4.1355	0.461518	3.5	482.946	137.985	13.832	1692591.881	0.0016	37.459	33.366
2.757	1.5	4.1355	0.461518	3.5	464.741	132.783	14.374	1692591.881	0.0016	38.927	32.108
2.757	1.5	4.1355	0.461518	6	464.741	77.457	24.641	1692591.881	0.0016	66.731	18.730
Room Temperature Carbon Fiber (25°C)											
2.757	1.5	4.1355	0.461518	3.5	468.335	133.810	14.264	1692591.881	0.0016	38.628	32.356
2.757	1.5	4.1355	0.461518	3.5	375.868	107.391	17.773	1692591.881	0.0016	48.131	25.968
2.757	1.5	4.1355	0.461518	3.5	500.765	143.076	13.340	1692591.881	0.0016	36.126	34.597
2.757	1.5	4.1355	0.461518	3.5	448.323	128.092	14.900	1692591.881	0.0016	40.352	30.974
2.757	1.5	4.1355	0.461518	6	448.323	74.720	25.543	1692591.881	0.0016	69.175	18.068
Temperature Gradient (-60°C / 25°C)											
2.757	1.5	4.1355	0.461518	3.5	496.067	141.733	13.466	1692591.881	0.0016	36.468	34.272
2.757	1.5	4.1355	0.461518	3.5	455.376	130.107	14.669	1692591.881	0.0016	39.727	31.461
2.757	1.5	4.1355	0.461518	3.5	475.566	135.876	14.047	1692591.881	0.0016	38.040	32.856
2.757	1.5	4.1355	0.461518	3.5	475.718	135.919	14.042	1692591.881	0.0016	38.028	32.866
2.757	1.5	4.1355	0.461518	3.5	475.682	135.909	14.043	1692591.881	0.0016	38.031	32.864
2.757	1.5	4.1355	0.461518	6	475.682	79.280	24.074	1692591.881	0.0016	65.196	19.171

Fuel Tank (Spherical)

-60°C Carbon Fiber

Pressure (MPa)	M.O.S	M.O.S Pressure (MPa)	Radius (m)	F.O.S	σ (UTS) (MPa)	σ (allow) (MPa)	t (mm)	Surface Area (mm^2)	Density (g/mm^3)	Weight (kg)	Thin Wall (r/t)>10
2.757	1.5	4.1355	0.461518	3.5	464.180	132.623	7.196	1338311.335	0.0016	15.408	64.139
2.757	1.5	4.1355	0.461518	3.5	447.096	127.742	7.471	1338311.335	0.0016	15.997	61.778
2.757	1.5	4.1355	0.461518	3.5	482.946	137.985	6.916	1338311.335	0.0016	14.809	66.732
2.757	1.5	4.1355	0.461518	3.5	464.741	132.783	7.187	1338311.335	0.0016	15.389	64.216
2.757	1.5	4.1355	0.461518	6	464.741	77.457	12.320	1338311.335	0.0016	26.382	37.459
Room Temperature Carbon Fiber (25°C)											
2.757	1.5	4.1355	0.461518	3.5	468.335	133.810	7.132	1338311.335	0.0016	15.271	64.713
2.757	1.5	4.1355	0.461518	3.5	375.868	107.391	8.886	1338311.335	0.0016	19.028	51.936
2.757	1.5	4.1355	0.461518	3.5	500.765	143.076	6.670	1338311.335	0.0016	14.282	69.194
2.757	1.5	4.1355	0.461518	3.5	448.323	128.092	7.450	1338311.335	0.0016	15.953	61.948
2.757	1.5	4.1355	0.461518	6	448.323	74.720	12.772	1338311.335	0.0016	27.348	36.136
Temperature Gradient (-60°C / 25°C)											
2.757	1.5	4.1355	0.461518	3.5	496.067	141.733	6.733	1338311.335	0.0016	14.418	68.545
2.757	1.5	4.1355	0.461518	3.5	455.376	130.107	7.335	1338311.335	0.0016	15.706	62.922
2.757	1.5	4.1355	0.461518	3.5	475.566	135.876	7.023	1338311.335	0.0016	15.039	65.712
2.757	1.5	4.1355	0.461518	3.5	475.718	135.919	7.021	1338311.335	0.0016	15.034	65.733
2.757	1.5	4.1355	0.461518	3.5	475.682	135.909	7.022	1338311.335	0.0016	15.035	65.728
2.757	1.5	4.1355	0.461518	6	475.682	79.280	12.037	1338311.335	0.0016	25.775	38.341

Oxidizer Tank (Cylindrical)											
-60°C Carbon Fiber											
Pressure (MPa)	M.O.S	M.O.S Pressure (MPa)	Radius (m)	F.O.S	σ (UTS) (MPa)	σ (allow) (MPa)	t (mm)	Surface Area (mm^2)	Density (g/mm^3)	Weight (kg)	Thin Wall (r/t)>10
2.757	1.5	4.1355	0.46355	3.5	464.180	132.623	14.455	1766625.492	0.0016	40.857	32.069
2.757	1.5	4.1355	0.46355	3.5	447.096	127.742	15.007	1766625.492	0.0016	42.419	30.889
2.757	1.5	4.1355	0.46355	3.5	482.946	137.985	13.893	1766625.492	0.0016	39.270	33.366
2.757	1.5	4.1355	0.46355	3.5	464.741	132.783	14.437	1766625.492	0.0016	40.808	32.108
2.757	1.5	4.1355	0.46355	6	464.741	77.457	24.749	1766625.492	0.0016	69.957	18.730
Room Temperature Carbon Fiber (25°C)											
2.757	1.5	4.1355	0.46355	3.5	468.335	133.810	14.326	1766625.492	0.0016	40.495	32.356
2.757	1.5	4.1355	0.46355	3.5	375.868	107.391	17.851	1766625.492	0.0016	50.457	25.968
2.757	1.5	4.1355	0.46355	3.5	500.765	143.076	13.399	1766625.492	0.0016	37.872	34.597
2.757	1.5	4.1355	0.46355	3.5	448.323	128.092	14.966	1766625.492	0.0016	42.303	30.974
2.757	1.5	4.1355	0.46355	6	448.323	74.720	25.656	1766625.492	0.0016	72.519	18.068
Temperature Gradient (-60°C / 25°C)											
2.757	1.5	4.1355	0.46355	3.5	496.067	141.733	13.525	1766625.492	0.0016	38.231	34.272
2.757	1.5	4.1355	0.46355	3.5	455.376	130.107	14.734	1766625.492	0.0016	41.647	31.461
2.757	1.5	4.1355	0.46355	3.5	475.566	135.876	14.109	1766625.492	0.0016	39.879	32.856
2.757	1.5	4.1355	0.46355	3.5	475.718	135.919	14.104	1766625.492	0.0016	39.866	32.866
2.757	1.5	4.1355	0.46355	3.5	475.682	135.909	14.105	1766625.492	0.0016	39.869	32.864
2.757	1.5	4.1355	0.46355	6	475.682	79.280	24.180	1766625.492	0.0016	68.348	19.171

Oxidizer Tank (Spherical)											
-60°C Carbon Fiber											
Pressure (MPa)	M.O.S	M.O.S Pressure (MPa)	Radius (m)	F.O.S	σ (UTS) (MPa)	σ (allow) (MPa)	t (mm)	Surface Area (mm^2)	Density (g/mm^3)	Weight (kg)	Thin Wall (r/t)>10
2.757	1.5	4.1355	0.46355	3.5	464.180	132.623	7.227	1350122.078	0.0016	15.612	64.139
2.757	1.5	4.1355	0.46355	3.5	447.096	127.742	7.503	1350122.078	0.0016	16.209	61.778
2.757	1.5	4.1355	0.46355	3.5	482.946	137.985	6.946	1350122.078	0.0016	15.006	66.732
2.757	1.5	4.1355	0.46355	3.5	464.741	132.783	7.219	1350122.078	0.0016	15.594	64.216
2.757	1.5	4.1355	0.46355	6	464.741	77.457	12.375	1350122.078	0.0016	26.732	37.459
Room Temperature Carbon Fiber (25°C)											
2.757	1.5	4.1355	0.46355	3.5	468.335	133.810	7.163	1350122.078	0.0016	15.474	64.713
2.757	1.5	4.1355	0.46355	3.5	375.868	107.391	8.925	1350122.078	0.0016	19.281	51.936
2.757	1.5	4.1355	0.46355	3.5	500.765	143.076	6.699	1350122.078	0.0016	14.472	69.194
2.757	1.5	4.1355	0.46355	3.5	448.323	128.092	7.483	1350122.078	0.0016	16.165	61.948
2.757	1.5	4.1355	0.46355	6	448.323	74.720	12.828	1350122.078	0.0016	27.711	36.136
Temperature Gradient (-60°C / 25°C)											
2.757	1.5	4.1355	0.46355	3.5	496.067	141.733	6.763	1350122.078	0.0016	14.609	68.545
2.757	1.5	4.1355	0.46355	3.5	455.376	130.107	7.367	1350122.078	0.0016	15.914	62.922
2.757	1.5	4.1355	0.46355	3.5	475.566	135.876	7.054	1350122.078	0.0016	15.239	65.712
2.757	1.5	4.1355	0.46355	3.5	475.718	135.919	7.052	1350122.078	0.0016	15.234	65.733
2.757	1.5	4.1355	0.46355	3.5	475.682	135.909	7.053	1350122.078	0.0016	15.235	65.728
2.757	1.5	4.1355	0.46355	6	475.682	79.280	12.090	1350122.078	0.0016	26.117	38.341

Appendix C

AS4/3501-6 (Axial)

Helium Tank (Spherical)											
Unidirectional (Axial)											
Pressure (MPa)	M.O.S	M.O.S Pressure (MPa)	Radius (m)	F.O.S	σ (UTS) (MPa)	σ (allow) (MPa)	t (mm)	Surface Area (mm^2)	Density (g/mm^3)	Weight (kg)	Thin Wall (r/t)>10
13.789	1.5	20.684	0.4445	3.5	2137.000	610.571	7.529	2482866.648	0.00152	28.414	59.039
13.789	1.5	20.684	0.4445	6	2137.000	356.167	12.907	2482866.648	0.00152	48.709	34.440

Fuel Tank (Cylindrical)											
Unidirectional (Axial)											
Pressure (MPa)	M.O.S	M.O.S Pressure (MPa)	Radius (m)	F.O.S	σ (UTS) (MPa)	σ (allow) (MPa)	t (mm)	Surface Area (mm^2)	Density (g/mm^3)	Weight (kg)	Thin Wall (r/t)>10
2.757	1.5	4.1355	0.461518	3.5	2137.000	610.571	3.126	1692591.881	0.00152	8.042	147.642
2.757	1.5	4.1355	0.461518	6	2137.000	356.167	5.359	1692591.881	0.00152	13.787	86.124
Fuel Tank (Spherical)											
Unidirectional (Axial)											
Pressure (MPa)	M.O.S	M.O.S Pressure (MPa)	Radius (m)	F.O.S	σ (UTS) (MPa)	σ (allow) (MPa)	t (mm)	Surface Area (mm^2)	Density (g/mm^3)	Weight (kg)	Thin Wall (r/t)>10
2.757	1.5	4.1355	0.461518	3.5	2137.000	610.571	1.563	1338311.335	0.00152	3.179	295.283
2.757	1.5	4.1355	0.461518	6	2137.000	356.167	2.679	1338311.335	0.00152	5.450	172.248

Oxidizer Tank (Cylindrical)											
Unidirectional (Axial)											
Pressure (MPa)	M.O.S	M.O.S Pressure (MPa)	Radius (m)	F.O.S	σ (UTS) (MPa)	σ (allow) (MPa)	t (mm)	Surface Area (mm^2)	Density (g/mm^3)	Weight (kg)	Thin Wall (r/t)>10
2.757	1.5	4.1355	0.46355	3.5	2137.000	610.571	3.140	1766625.492	0.00152	8.431	147.642
2.757	1.5	4.1355	0.46355	6	2137.000	356.167	5.382	1766625.492	0.00152	14.453	86.124
Oxidizer Tank (Spherical)											
Unidirectional (Axial)											
Pressure (MPa)	M.O.S	M.O.S Pressure (MPa)	Radius (m)	F.O.S	σ (UTS) (MPa)	σ (allow) (MPa)	t (mm)	Surface Area (mm^2)	Density (g/mm^3)	Weight (kg)	Thin Wall (r/t)>10
2.757	1.5	4.1355	0.46355	3.5	2137.000	610.571	1.570	1350122.078	0.00152	3.222	295.283
2.757	1.5	4.1355	0.46355	6	2137.000	356.167	2.691	1350122.078	0.00152	5.523	172.248

Appendix D

AS4/3501-6 (Transverse)

Helium Tank (Spherical)											
Unidirectional (Transverse)											
Pressure (MPa)	M.O.S	M.O.S Pressure (MPa)	Radius (m)	F.O.S	σ (UTS) (MPa)	σ (allow) (MPa)	t (mm)	Surface Area (mm^2)	Density (g/mm^3)	Weight (kg)	Thin Wall (r/t)>10
13.789	1.5	20.684	0.4445	3.5	53.400	15.257	301.295	2482866.648	0.00152	1137.076	1.475
13.789	1.5	20.684	0.4445	6	53.400	8.900	516.507	2482866.648	0.00152	1949.273	0.861

Fuel Tank (Cylindrical)											
Unidirectional (Transverse)											
Pressure (MPa)	M.O.S	M.O.S Pressure (MPa)	Radius (m)	F.O.S	σ (UTS) (MPa)	σ (allow) (MPa)	t (mm)	Surface Area (mm^2)	Density (g/mm^3)	Weight (kg)	Thin Wall (r/t)>10
2.757	1.5	4.1355	0.461518	3.5	53.400	15.257	125.096	1692591.881	0.00152	321.839	3.689
2.757	1.5	4.1355	0.461518	6	53.400	8.900	214.450	1692591.881	0.00152	551.725	2.152
Fuel Tank (Spherical)											
Unidirectional (Transverse)											
Pressure (MPa)	M.O.S	M.O.S Pressure (MPa)	Radius (m)	F.O.S	σ (UTS) (MPa)	σ (allow) (MPa)	t (mm)	Surface Area (mm^2)	Density (g/mm^3)	Weight (kg)	Thin Wall (r/t)>10
2.757	1.5	4.1355	0.461518	3.5	53.400	15.257	62.548	1338311.335	0.00152	127.237	7.379
2.757	1.5	4.1355	0.461518	6	53.400	8.900	107.225	1338311.335	0.00152	218.121	4.304

Oxidizer Tank (Cylindrical)											
Unidirectional (Transverse)											
Pressure (MPa)	M.O.S	M.O.S Pressure (MPa)	Radius (m)	F.O.S	σ (UTS) (MPa)	σ (allow) (MPa)	t (mm)	Surface Area (mm^2)	Density (g/mm^3)	Weight (kg)	Thin Wall (r/t)>10
2.757	1.5	4.1355	0.46355	3.5	53.400	15.257	125.647	1766625.492	0.00152	337.396	3.689
2.757	1.5	4.1355	0.46355	6	53.400	8.900	215.394	1766625.492	0.00152	578.393	2.152
Oxidizer Tank (Spherical)											
Unidirectional (Transverse)											
Pressure (MPa)	M.O.S	M.O.S Pressure (MPa)	Radius (m)	F.O.S	σ (UTS) (MPa)	σ (allow) (MPa)	t (mm)	Surface Area (mm^2)	Density (g/mm^3)	Weight (kg)	Thin Wall (r/t)>10
2.757	1.5	4.1355	0.46355	3.5	53.400	15.257	62.823	1350122.078	0.00152	128.925	7.379
2.757	1.5	4.1355	0.46355	6	53.400	8.900	107.697	1350122.078	0.00152	221.015	4.304

Appendix E

AL 2219 T87

Helium Tank (Spherical)											
Pressure (MPa)	M.O.S	M.O.S Pressure (MPa)	Radius (m)	F.O.S	σ (UTS) (MPa)	σ (allow) (MPa)	t (mm)	Surface Area (mm^2)	Density (g/mm^3)	Weight (kg)	Thin Wall (r/t)>10
13.789	1.5	20.684	0.4445	2.5	476.000	190.400	24.143	2482866.648	0.00284	170.244	18.411

Fuel Tank (Cylindrical)											
Pressure (MPa)	M.O.S	M.O.S Pressure (MPa)	Radius (m)	F.O.S	σ (UTS) (MPa)	σ (allow) (MPa)	t (mm)	Surface Area (mm^2)	Density (g/mm^3)	Weight (kg)	Thin Wall (r/t)>10
2.757	1.5	4.1355	0.461518	2.5	476.000	190.400	10.024	1692591.881	0.00284	48.186	46.040
Fuel Tank (Spherical)											
Pressure (MPa)	M.O.S	M.O.S Pressure (MPa)	Radius (m)	F.O.S	σ (UTS) (MPa)	σ (allow) (MPa)	t (mm)	Surface Area (mm^2)	Density (g/mm^3)	Weight (kg)	Thin Wall (r/t)>10
2.757	1.5	4.1355	0.461518	2.5	476.000	190.400	5.012	1338311.335	0.00284	19.050	92.081

Oxidizer Tank (Cylindrical)											
Pressure (MPa)	M.O.S	M.O.S Pressure (MPa)	Radius (m)	F.O.S	σ (UTS) (MPa)	σ (allow) (MPa)	t (mm)	Surface Area (mm^2)	Density (g/mm^3)	Weight (kg)	Thin Wall (r/t)>10
2.757	1.5	4.1355	0.46355	2.5	476.000	190.400	10.068	1766625.492	0.00284	50.515	46.040
Oxidizer Tank (Spherical)											
Pressure (MPa)	M.O.S	M.O.S Pressure (MPa)	Radius (m)	F.O.S	σ (UTS) (MPa)	σ (allow) (MPa)	t (mm)	Surface Area (mm^2)	Density (g/mm^3)	Weight (kg)	Thin Wall (r/t)>10
2.757	1.5	4.1355	0.46355	2.5	476.000	190.400	5.034	1350122.078	0.00284	19.303	92.081

Curriculum Vitae

Itzel Torres was born on September 23,1995 in El Paso, Texas. She began college at The University of Texas at El Paso in the Fall of 2014. She began working as an undergraduate research assitant at The Center for Space Exploration and Technology Research (cSETR) while pursuing her bachelor's degree in mechanical engineering. In the summer of 2018, she entered the Graduate School at the University of Texas at El Paso, where she has earned a Master's degree in Mechanical Engineering. She continued to work for cSETR now as a graduate research assistant while pursuing her master's degree. Her research included the design of a small payload launch vehicle, failure mechanisms of composite materials, and the design of a condensder chamber for ice deposition measurement.

Permanent address: 11009 Dragonfly Way
El Paso, Texas 79936